1 INTRODUCTION 3

2 AQUEOUS CO_2 CORROSION OF MILD STEEL 3

2.1 CHEMISTRY OF CO_2 SATURATED AQUEOUS SOLUTIONS – EQUILIBRIUM CONSIDERATIONS 4

2.2 ELECTROCHEMISTRY OF MILD STEEL CORROSION IN CO_2 SATURATED AQUEOUS SOLUTIONS 12

2.2.1 Oxidation of iron 16

2.2.2 Reduction of hydronium ion 16

2.2.3 Reduction of carbonic acid 18

2.2.4 Reduction of acetic acid 20

2.2.5 Reduction of oxygen 22

2.2.6 Reduction of water 23

2.3 TRANSPORT PROCESSES IN CO_2 CORROSION OF MILD STEEL 24

2.4 CALCULATION OF MILD STEEL CO_2 CORROSION RATE 27

2.5 SUCCESSES AND LIMITATIONS OF MODELING OF AQUEOUS CO_2 CORROSION OF MILD STEEL 28

2.6 KEY FACTORS AFFECTING AQUEOUS CO_2 CORROSION OF MILD STEEL 30

2.6.1 The effect of pH 30

2.6.2 The effect of CO_2 partial pressure 31

2.6.3 The effect of temperature 33

2.6.4 The effect of flow 34

2.6.5 Effect of corrosion inhibition 38

2.6.6 The effect of organic acids 39

2.6.7 Effect of glycol/methanol 40

2.6.8 Effect of condensation in wet gas flow 41

2.6.9 Non-ideal solutions and gases 41

2.7 LOCALIZED CO_2 CORROSION OF MILD STEEL IN AQUEOUS SOLUTIONS 42

3 AQUEOUS H_2S CORROSION OF MILD STEEL 43

3.1 CHEMISTRY OF H_2S SATURATED AQUEOUS SOLUTIONS – EQUILIBRIUM CONSIDERATIONS 44

3.2 MILD STEEL CORROSION IN H_2S AND MIXED H_2S/CO_2/HAC SATURATED AQUEOUS SOLUTIONS 53

3.3 CALCULATION OF MILD STEEL H_2S CORROSION RATE 56

3.3.1 Pure H_2S aqueous environment 56

3.3.2 Mixed CO_2/H_2S Environments 60

3.3.3 Mixed $CO_2 / HAc / H_2S$ Environments 61

3.4 LIMITATIONS OF MODELING OF AQUEOUS H_2S CORROSION OF MILD STEEL 62

3.5 KEY FACTORS AFFECTING AQUEOUS H_2S CORROSION OF MILD STEEL 63

3.5.1 Effect of H_2S partial pressure 63

3.5.2 Effect of time 68

3.6 LOCALIZED H_2S CORROSION OF MILD STEEL IN AQUEOUS SOLUTIONS 72

4 NOMENCALTURE 73

5 REFERENCES 82

1 INTRODUCTION

As the oil and gas emerge from the geological formation they are always accompanied by some water and varying amounts of "acid gases": carbon dioxide, CO_2 and hydrogen sulfide, H_2S. This is a corrosive combination which affects the integrity of mild steel. Even if this has been known for over 100 years, yet aqueous CO_2 and H_2S corrosion of mild steel still represents a significant problem for the oil and gas industry.[1] Although corrosion resistance alloys exist that are able to withstand this type of corrosion, mild steel is still the most cost effective construction material used in this industry for these applications. All of the pipelines, many wells and much of the processing equipment in the oil and gas industry are built out of mild steel. The cost of equipment failure due to internal CO_2/H_2S corrosion is enormous, both in terms of direct costs such as: repair costs and lost production, as well as in indirect costs such as: environmental cost, impact on the downstream industries, etc.

The text below summarizes the degree of understanding of the so-called "sweet" CO_2 corrosion and the so-called "sour" or H_2S corrosion of mild steel exposed to aqueous environments. It also casts the knowledge in the form of mathematical equations whenever possible. This should enable corrosion engineers and scientists to build entry level corrosion simulation and prediction models.

2 AQUEOUS CO_2 CORROSION OF MILD STEEL

Aqueous CO_2 corrosion of carbon steel is an electrochemical process involving the anodic dissolution of iron and the cathodic evolution of hydrogen. The overall reaction is:

$$Fe + CO_2 + H_2O \rightarrow FeCO_3 + H_2 \quad (1)$$

CO_2 corrosion of mild steel is reasonably well understood. A number of chemical, electrochemical and transport processes occur simultaneously. They are briefly described below.

2.1 Chemistry of CO_2 Saturated Aqueous Solutions – Equilibrium Considerations

The CO_2 gas is soluble in water:

$$CO_{2(g)} \overset{K_{sol}}{\Leftrightarrow} CO_2 \quad (2)$$

For ideal gases and ideal solutions in equilibrium, Henry's law can be used to calculate the aqueous concentration of dissolved CO_2, c_{CO_2}, given that the respective concentration in the gas phase (often expressed in terms of partial pressure, p_{CO_2}) is known:

$$H_{sol(CO_2)} = \frac{1}{K_{sol(CO_2)}} = \frac{p_{CO_2}}{c_{CO_2}} \quad (3)$$

The CO_2 solubility constant, $K_{sol(CO_2)}$, is a function of temperature, T_f, and ionic strength, I:[2]

$$K_{sol(CO_2)} = \frac{14.5}{1.00258} 10^{-(2.27+5.65\times10^{-3}T_f - 8.06\times10^{-6}T_f^2 + 0.075I)} \quad (4)$$

Ionic strength, I , can be calculated as:

$$I = \frac{1}{2}\sum_i c_i z_i^2 = \frac{1}{2}\left(c_1 z_1^2 + c_2 z_2^2 + \ldots\right) \tag{5}$$

The concentration of CO_2 in the aqueous phase is of the same order of magnitude as the one in the gas phase. For example at p_{CO_2} =1 bar, at 25°C, the gaseous CO_2 concentration is approximately 4 mol/l (kmol/m^3) while in the water it is about 3 mol/l. Since the solubility of CO_2 decreases with temperature, at 100°C the respective concentrations are: 3.3 mol/l in the gas and 1.1 mol/l in the water.

A rather small fraction (about one in five hundred) of the dissolved CO_2 molecules hydrates to make a "weak" carbonic acid, H_2CO_3 :

$$CO_2 + H_2O \overset{K_{hy}}{\Leftrightarrow} H_2CO_3 \tag{6}$$

due to a relatively slow forward (hydration) rate. Assuming that the concentration of water remains unchanged, the equilibrium concentration $c_{H_2CO_3}$ is determined by:

$$K_{hyd} = \frac{c_{H_2CO_3}}{c_{CO_2}} \tag{7}$$

The equilibrium hydration/dehydration constant, $K_{hyd} = 2.58 \cdot 10^{-3}$, does not change much across the typical temperature range of interest (20 – 100°C).[3]

Carbonic acid is considered to be "weak" because it only partially dissociates to produce hydronium, H^+ ions and bicarbonate ion, HCO_3^-:

$$H_2CO_3 \overset{K_{ca}}{\Leftrightarrow} H^+ + HCO_3^- \tag{8}$$

The HCO_3^- dissociates further to give some more H^+ and carbonate ion, CO_3^{2-}:

$$HCO_3^- \overset{K_{bi}}{\Leftrightarrow} H^+ + CO_3^{2-} \tag{9}$$

The respective equilibrium relations can be written as:

$$K_{ca} = \frac{c_{H^+} c_{HCO_3^-}}{c_{H_2CO_3}} \tag{10}$$

$$K_{bi} = \frac{c_{H^+} c_{CO_3^{2-}}}{c_{HCO_3^-}} \tag{11}$$

The equilibrium constants can be calculated as functions of temperature, T_f, and ionic strength, I, as:[2]

$$K_{ca} = 387.6 \cdot 10^{-\left(6.41 - 1.594 \cdot 10^{-3} T_f + 8.52 \cdot 10^{-6} T_f^2 - 3.07 \cdot 10^{-5} p_{CO_2} \cdot 14.5 - 0.4772 \cdot I^{0.5} + 0.118 \cdot I\right)} \tag{12}$$

$$K_{bi} = 10^{-\left(10.61 - 4.97 \cdot 10^{-3} T_f + 1.331 \cdot 10^{-5} T_f^2 - 2.624 \cdot 10^{-5} p_{CO_2} \cdot 14.5 - 1.166 \cdot I^{0.5} + 0.3466 \cdot I\right)} \tag{13}$$

The low molecular weight organic acids are primarily soluble in water and can lead to corrosion of mild steel. Higher molecular weight organic acids are not water soluble but are typically soluble in the oil phase and pose a corrosion threat at higher temperatures in the refineries. Acetic acid CH_3COOH (denoted as *HAc* in the text below) is the most prevalent low molecular weight organic acid found in brines. Other acids typically found in the brine are propionic, formic, etc., however their behavior and corrosiveness is very similar to that of *HAc* and therefore *HAc* can be used as a "surrogate" for all the organic acids found in the brine. *HAc* is a weak acid, however it is stronger than H_2CO_3 (pKa 4.76 vs 6.35 at 25°C), and it is the main source of H^+ ions when the two acid concentrations are similar.

The dissociation of aqueous *HAc*:

$$HAc \Leftrightarrow H^+ + Ac^- \tag{14}$$

is relatively fast, but proceeds only partially i.e. aqueous *HAc* is also a "weak" acid, just like H_2CO_3 discussed above. The pH i.e. the concentration of hydrogen ions, $[H^+]$, determines the distribution of the acetic species in the solution.

The equilibrium constant associated with dissociation of *HAc* is a function of temperature and can be calculated as:

$$K_{HAc} = 10^{-\left(6.66104 - 0.0134916 \cdot T_K + 2.37856 \cdot 10^{-5} \cdot T_K^2\right)} \tag{15}$$

The dissociation steps (8) and (9) are very fast compared to all other processes occurring simultaneously in corrosion of mild steel, thus preserving chemical equilibrium. However, the CO_2 dissolution reaction (2) and the hydration reaction (6) are much slower. When such chemical reactions proceed slowly, other faster processes (such as electrochemical reactions or diffusion) can lead to local non-equilibrium in the solution.

Either way, the occurrence of chemical reactions can significantly alter the rate of electrochemical processes at the surface and the rate of corrosion. This is particularly true when, due to high local concentrations of species, the solubility limit of salts is exceeded and precipitation of a surface layer occurs. In a precipitation process, heterogeneous nucleation occurs first on the surface of the metal or within the pores of an existing layer since homogenous nucleation in the bulk requires a much higher concentration of species. Nucleation is followed by crystalline layer growth. Under certain conditions surface layers can become very protective and reduce the rate of corrosion.

In CO_2 corrosion when the concentrations of Fe^{2+} and CO_3^{2-} ions exceed the solubility limit, they form solid ferrous carbonate according to:

$$Fe^{2+} + CO_3^{2-} \overset{K_{sp(FeCO_3)}}{\Leftrightarrow} FeCO_{3(s)} \tag{16}$$

where the solubility product constant for ferrous carbonate $K_{sp(FeCO_3)}$ is:[4]

$$K_{sp(FeCO_3)} = 10^{-59.3498 - 0.041377 \cdot T_k - \frac{2.1963}{T_k} + 24.5724 \cdot \log T_k + 2.518 \cdot I^{0.5} - 0.657 \cdot I} \quad (17)$$

Actually ferrous carbonate is frequently found in the aqueous solution at concentrations much higher than predicted by the equilibrium $K_{sp(FeCO_3)}$. This is termed *supersaturation* and is a necessary condition before any substantial precipitation can occur. The ferrous carbonate supersaturation, $SS_{(FeCO_3)}$ is defined as:

$$SS_{(FeCO_3)} = \frac{c_{Fe^{2+}} c_{CO_3^{2-}}}{K_{sp(FeCO_3)}} \quad (18)$$

The precipitation process can be seen as the process of the solution returning to equilibrium and is driven by the magnitude of supersaturation. The rate of precipitation ($\Re_{FeCO_3}$) is therefore often expressed as:

$$\Re_{FeCO_3} = k_{r(FeCO_3)} \frac{A}{V} K_{sp(FeCO_3)} \left(SS_{(FeCO_3)} - 1 \right) \quad (19)$$

where $k_{r(FeCO_3)}$ is a kinetics constant, which can be derived from the experimental results as a function of temperature, using an Arrhenius's type equation:[5]

$$k_{r(FeCO_3)} = e^{A_{(FeCO_3)} - \frac{B_{(FeCO_3)}}{RT_k}} \quad (20)$$

where $A_{(FeCO_3)}$ =21.3 and $B_{(FeCO_3)}$ 64,851.4 J/mol.

Images of a crystalline ferrous carbonate layer formed on a mild steel substrate are shown in Figure. The ferrous carbonate layer can slow down the corrosion process by presenting a diffusion barrier for the species involved in the corrosion process and thereby changing the conditions at the steel surface. The effective protectiveness of a solid ferrous carbonate layer depends on its porosity which hangs in the balance of the precipitation rate and the underlying corrosion rate. For high precipitation rates, and low corrosion rates, a dense and protective ferrous carbonate layer is obtained and vice versa, low precipitation rates and high corrosion rates lead to formation of porous unprotective ferrous carbonate layers. A non-dimensional parameter termed "scaling tendency" (ST) can be used to quantify the relative rates of precipitation ($\Re_{FeCO_3}$) and corrosion (CR) expressed in the same volumetric units:

$$ST = \frac{\Re_{FeCO_3}}{CR} \tag{21}$$

For ST <<1, porous and unprotective films are likely to form. Conversely, for $ST \geq 1$, conditions become favourable for formation of dense, protective ferrous carbonate films. However, the use of scaling tendency is not as straightforward as it appears, as it requires simultaneous calculation of $\Re_{FeCO_3}$ and corrosion CR.

In some cases other salts can be detected in the surface layers that form on mild steel. In high temperature CO_2 corrosion magnetite (Fe_3O_4) has been detected. In the presence of oxygen a ferric oxide hematite (Fe_2O_3) forms which is very insoluble but offers little protection from corrosion. Finally, in the presence of H_2S, various types of sulfides form as discussed in a separate chapter below.

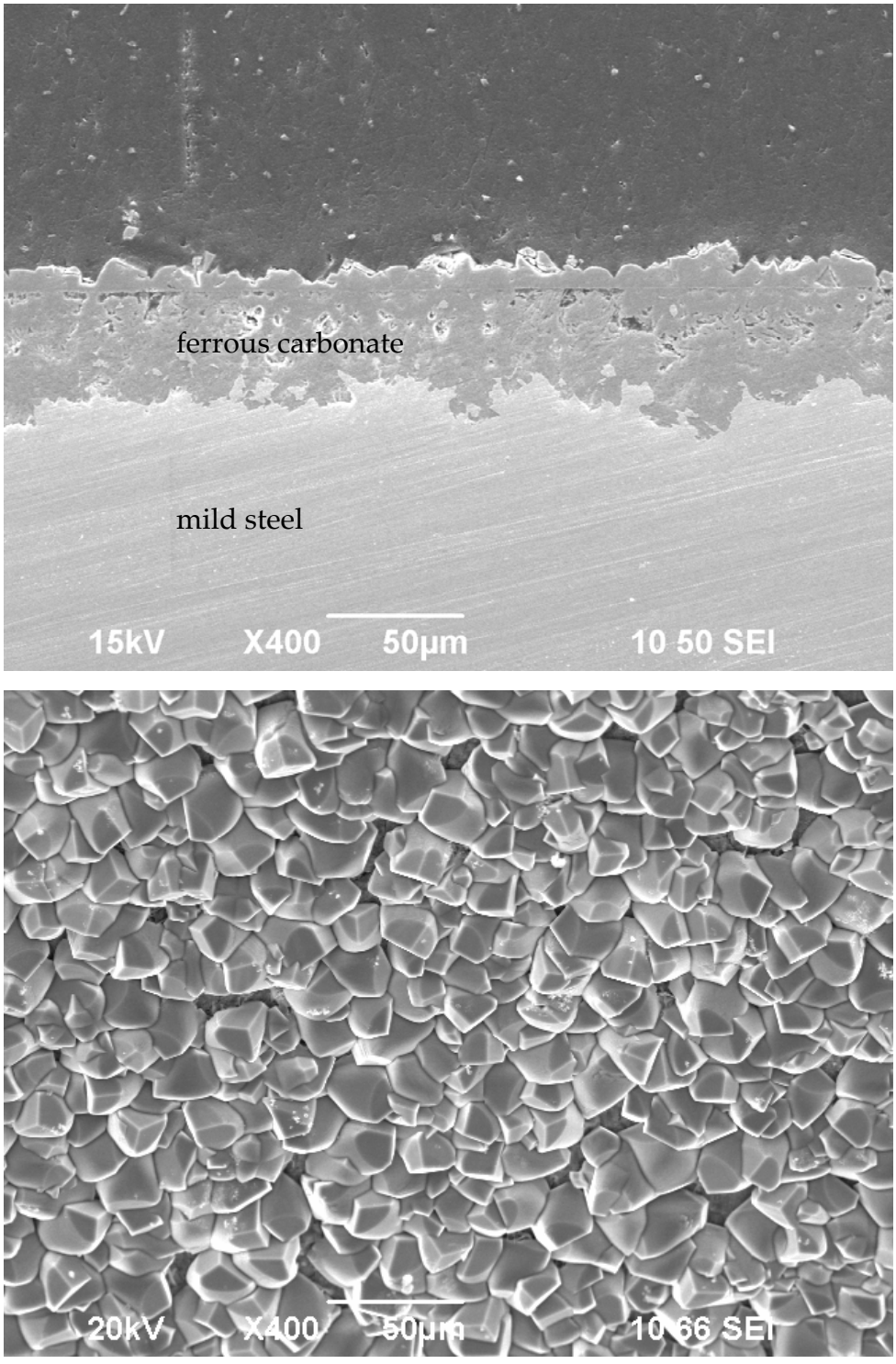

Figure 1. A cross section and a top view of a ferrous carbonate layer formed on mild steel; 80°C, pH6.6, p_{CO_2} =0.5 bar, stagnant conditions.

2.2 Electrochemistry of Mild Steel Corrosion in CO_2 Saturated Aqueous Solutions

The electrochemical dissolution of iron in a water solution:

$$Fe \rightarrow Fe^{2+} + 2e^{-} \tag{22}$$

is the dominant anodic reaction in CO_2 corrosion. The reaction is pH dependent in acidic solutions with a reaction order with respect to OH^- between 1 and 2, decreasing toward 1 and 0 at pH >4, which is the typical range for CO_2 corrosion. Measured Tafel slopes are typically 30-80 mV. This subject, which is still somewhat controversial with respect to the mechanism, has been reviewed for acidic corrosion[6,7] and CO_2 solutions.[8]

The presence of CO_2 increases the rate of corrosion of mild steel in aqueous solutions primarily by increasing the rate of the hydrogen evolution reaction. It is well known that in *strong* acids, which are fully dissociated, the rate of hydrogen evolution occurs according to:

$$2H^{+} + 2e^{-} \rightarrow H_2 \tag{23}$$

and is, for the case of mild steel corrosion, limited by the rate at which H^+ ions are transported from the bulk solution to the steel surface (mass transfer limitation). In CO_2 solutions where typically pH>4, this limiting flux would be small and therefore it is the presence of H_2CO_3 which enables hydrogen evolution at a much higher rate.

Thus for pH>4 the presence of CO_2 leads to a much higher corrosion rate than would be found in a solution of a *strong* acid at the same pH.

This can be readily explained by considering that the homogenous dissociation of H_2CO_3, as given by reaction (8), serves as an additional source of H^+ ions, which are subsequently adsorbed at the steel surface and reduced according to reaction (23).[1] A different pathway is also possible, where the H_2CO_3 first adsorbs at the steel surface followed by heterogeneous dissociation and reduction of the H^+ ion. This is often referred to as "direct" reduction of carbonic acid[9, 10, 11] and is written as:

$$2H_2CO_3 + 2e^- \rightarrow H_2 + 2HCO_3^- \qquad (24)$$

Clearly the addition of reactions (8) and (23) gives reaction (24) proving that the overall reaction is the same and the distinction is only in the pathway, i.e in the sequence of reactions. The rate of reaction (24) is limited primarily by the slow hydration step (6) [11, 12] and in some cases by the slow CO_2 dissolution reaction (2).

It can be conceived that in CO_2 solutions at pH>5 the direct reduction of the bicarbonate ion becomes important: [13]

$$2HCO_3^- + 2e^- \rightarrow H_2 + 2CO_3^{2-} \qquad (25)$$

what seems plausible, as the concentration of HCO_3^- increases with pH and can exceed that of H_2CO_3 as seen in Figure 2. However it is difficult to experimentally

distinguish the effect of this particular reaction pathway for hydrogen evolution from the two previously discussed ((23 and (24). In addition evidence exists which suggests that the rate of this reaction is comparatively low and can be neglected. For example: as the pH increases, the amount of HCO_3^- increases as well (see Figure 2), suggesting that the corrosion rate should follow the same trend, if one is to believe that the direct reduction of the bicarbonate ion (25) is a significant cathodic reaction. Experimental evidence does not support this scenario and shows the opposite trend: the corrosion rate actually decreases with an increasing pH, even if no protective ferrous carbonate layer forms.

Acetic acid is well known to be one of the species that attacks mild steel. It was clearly established that the main cause of mild steel corrosion is the undissociated ("free") HAc and not the acetate ion Ac^-.[20] Therefore the presence of organic acids is a major corrosion concern particularly at lower pH, and particularly at high temperature.

Being a weak i.e. partially dissociated acid, HAc can be seen as an additional source of H^+, which are then adsorbed at the steel surface and reduced according to the cathodic reaction (23). It is also possible that HAc molecule itself is adsorbed at the steel surface followed by the heterogeneous reduction of H^+, which is often referred to as the "direct HAc reduction" pathway:

$$2HAc + 2e^- \rightarrow H_2 + 2Ac^- \qquad (26)$$

Although oxygen is not common corrosive specie in oil and gas pipeline system, it could invade the system by inappropriate operation or incomplete de-oxidation of

water chemical solutions injected into the system. Therefore, oxygen is likely to exist in oil and gas pipelines. Oxygen can contribute to corrosion process by an oxygen reduction reaction as shown below:

$$O_2 + 2H_2O + 4e^- \rightarrow 4OH^- \tag{27}$$

Hydrogen evolution by direct reduction of water:

$$2H_2O + 2e^- \rightarrow H_2 + 2OH^- \tag{28}$$

is always possible, but is comparatively very slow and is important only at p_{CO_2} <<0.1 bar and pH>6.[14, 15] Therefore this reaction is rarely a factor in practical CO_2 corrosion situations.

The various electrochemical processes described above can be quantified using the well established electrochemical theory. The rate of the electrochemical reactions, $\Re$ in kmol/(m^2 s), can be readily expressed in terms of current density, i in A/m^2, since the two are directly related: for example during hydrogen evolution (23) for every kmol of H^+ one kmol of electrons is used (n=1 kmol$_e$/kmol), while for every kmol of iron dissolved (22) two kmoles of electrons are used (n=2 kmol$_e$/kmol). Therefore one can write:

$$i = nF\Re \tag{29}$$

2.2.1 Oxidation of iron

In corrosion of mild steel, the oxidation (dissolution) of iron (22) is the dominant anodic reaction. The anodic dissolution of iron at the corrosion potential (and up to 200 mV above) is under charge transfer control. Thus, pure Tafel behavior can be assumed close to the corrosion potential:

$$i_{a(Fe)} = i_{o(Fe)}\, 10^{\frac{E_{corr} - E_{rev(Fe)}}{b_{a(Fe)}}} \tag{30}$$

The temperature dependence of exchange current density of iron oxidation is a function of temperature:

$$i_{o(Fe)} = i_{o(Fe)}^{ref}\, e^{\frac{-\Delta H_{Fe}}{R}\left(\frac{1}{T_c + 273.15} - \frac{1}{T_{c,ref} + 273.15}\right)} \tag{31}$$

The Tafel slope of this reaction is given by:

$$b_{a(Fe)} = \frac{2.303\, R\left(T_c + 273.15\right)}{1.5\, F} \tag{32}$$

2.2.2 Reduction of hydronium ion

In general, the H^+ reduction reaction (23) can be either under charge transfer or mass transfer (diffusion) control, therefore one can write:

$$\frac{1}{i_{c\left(H^+\right)}} = \frac{1}{i_{\alpha\left(H^+\right)}} + \frac{1}{i^{d}_{\lim\left(H^+\right)}} \tag{33}$$

The charge transfer current density can be calculated by:

$$i_{\alpha(H^+)} = i_{o(H^+)} \cdot 10^{-\frac{E_{corr} - E_{rev(H^+)}}{b_{c(H^+)}}} \tag{34}$$

The exchange current density $i_{o(H^+)}$ is a function of pH and temperature. The pH dependence is:

$$\frac{\partial \log i_{o(H^+)}}{\partial pH} = -0.5 \tag{35}$$

The temperature dependence of the exchange current density can be calculated via an Arrhenius-type relation:

$$\frac{i_{o(H^+)}}{i_{o(H^+)}^{ref}} = e^{-\frac{\Delta H_{(H^+)}}{R}\left(\frac{1}{T_c + 273.15} - \frac{1}{T_{c,ref} + 273.15}\right)} \tag{36}$$

The reversible potential for H^+ reduction $E_{rev(H^+)}$ is a function of temperature and pH:

$$E_{rev(H^+)} = -\frac{2.303\ R\left(T_c + 273.15\right)}{F} pH \tag{37}$$

The cathodic Tafel slope $b_{c(H^+)}$ is calculated as:

$$b_{c(H^+)} = \frac{2.303\ R\left(T_c + 273.15\right)}{0.5\ F} \tag{38}$$

The limiting mass transfer current density $i^{d}_{\lim(H^+)}$ is related to the rate of transport of H^+ ions form the bulk of the solution through the boundary layer to the steel surface:

$$i^{d}_{\lim(H^+)} = k_{m(H^+)} F\ c_{H^+} \tag{39}$$

where the mass transfer coefficient, $k_{m(H^+)}$ can be calculated from a correlation of the Sherwood, Reynolds, and Schmidt numbers as explained in the following section.

2.2.3 Reduction of carbonic acid

The carbonic acid reduction reaction (24) can be under charge transfer control or limited by the slow chemical reaction – hydration step (6), preceding it.[11, 12] The rate of this reaction in terms of current density is:

$$\frac{1}{i_{c(H_2CO_3)}} = \frac{1}{i_{\alpha(H_2CO_3)}} + \frac{1}{i^{r}_{\lim(H_2CO_3)}} \tag{40}$$

The charge transfer current density $i_{\alpha(H_2CO_3)}$ is calculated as:

$$i_{\alpha(H_2CO_3)} = i_{o(H_2CO_3)} \cdot 10^{-\frac{E_{corr} - E_{rev(H_2CO_3)}}{b_{c(H_2CO_3)}}} \tag{41}$$

The exchange current density $i_{o(H_2CO_3)}$ depends on pH, H_2CO_3 concentration, and temperature:

$$\frac{\partial \log i_{o(H_2CO_3)}}{\partial pH} = 0.5 \tag{42}$$

$$\frac{\partial \log i_{o(H_2CO_3)}}{\partial c_{H_2CO_3}} = 1 \tag{43}$$

$$\frac{i_{o(H_2CO_3)}}{i^{ref}_{o(H_2CO_3)}} = e^{-\frac{\Delta H_{(H_2CO_3)}}{R}\left(\frac{1}{T_c + 273.15} - \frac{1}{T_{c,ref} + 273.15}\right)} \tag{44}$$

The cathodic Tafel slope $b_{c(H_2CO_3)}$ is:

$$b_{c(H_2CO_3)} = \frac{2.303\ R\left(T_c + 273.15\right)}{0.5\ F} \tag{45}$$

Since the reduction of H_2CO_3 and H^+ are equivalent thermodynamically, the reversible potential for H_2CO_3 reduction $E_{rev(H_2CO_3)}$ is calculated as:

$$E_{rev(H_2CO_3)} = -\frac{2.303\ R\left(T_c + 273.15\right)}{F} pH \tag{46}$$

The chemical reaction limiting current density $i^r_{\lim(H_2CO_3)}$ can be calculated from: [16]

$$i^r_{\lim(H_2CO_3)} = F\ c_{CO_2}\ f_{H_2CO_3}\ \sqrt{D_{H_2CO_3} K_{hyd} k^f_{hyd}} \tag{47}$$

The diffusion coefficient for carbonic acid $D_{H_2CO_3}$ as a function of temperature can be calculated using Einstein's relation:

$$D = D_{ref}\left(\frac{T_c + 273.15}{T_{c,ref} + 273.15}\right)\left(\frac{\mu_{H_2O,ref}}{\mu_{H_2O}}\right) \tag{48}$$

The forward reaction rate for the CO_2 hydration reaction k_{hyd}^{f} is calculated as:

$$k_{hyd}^{f} = 10^{169.2 - 53.0 \cdot \log(T_c + 273.15) - \frac{11,715}{T_c + 273.15}} \tag{49}$$

The flow factor $f_{H_2CO_3}$ is:

$$f_{H_2CO_3} = \coth \zeta_{H_2CO_3} \tag{50}$$

where

$$\zeta_{H_2CO_3} = \frac{\delta_{m(H_2CO_3)}}{\delta_{r(H_2CO_3)}} \tag{51}$$

and

$$\delta_{m(H_2CO_3)} = \frac{D_{H_2CO_3}}{k_{m(H_2CO_3)}} \tag{52}$$

$$\delta_{r(H_2CO_3)} = \sqrt{\frac{D_{H_2CO_3}}{k_{hyd}^{b}}} \tag{53}$$

The carbonic acid mass transfer coefficient $k_{m(H_2CO_3)}$ is discussed in the following section 2.3.

2.2.4 Reduction of acetic acid

The acetic acid reduction reaction (26) can be either under charge transfer or mass transfer (diffusion) control, therefore acetic acid reduction rate can be calculated as:

$$\frac{1}{i_{c(HAc)}} = \frac{1}{i_{\alpha(HAc)}} + \frac{1}{i^{d}_{\lim(HAc)}} \tag{54}$$

The charge transfer current density is given as:

$$i_{\alpha(HAc)} = i_{o(HAc)} \cdot 10^{-\frac{E_{corr} - E_{rev(HAc)}}{b_{c(HAc)}}} \tag{55}$$

The exchange current density of this reaction are functions of undissociated *HAc* concentration and temperature, which can be obtained from,

$$i_{o(HAc)} = i^{ref}_{o(HAc)} \cdot \left(\frac{c_{HAc}}{c_{HAc,ref}} \right)^{0.5} \cdot e^{\frac{-\Delta H_{HAc}}{R}\left(\frac{1}{T_c + 273.15} - \frac{1}{T_{c,ref} + 273.15} \right)} \tag{56}$$

The reversible potential and Tafel slope of this reaction are obtained using the same equations as those for H^+ reduction:

$$E_{rev(HAc)} = -\frac{2.303\ R\left(T_c + 273.15\right)}{F}\, pH \tag{57}$$

$$b_{c(HAc)} = \frac{2.303\ R\left(T_c + 273.15\right)}{0.5\ F} \tag{58}$$

The mass transfer limiting current density $i^{d}_{\lim(HAc)}$ is given by,

$$i^{d}_{\lim(HAc)} = k_{m(HAc)} F c_{HAc} \tag{59}$$

Again, the mass transfer coefficient $k_{m(HAc)}$ can be calculated using the correlation described in the later section.

2.2.5 Reduction of oxygen

Like H^+ and HAc, oxygen reduction can be either charge transfer control or mass transfer control, therefore, the current density is calculated as the sum of two portions, charge transfer current density and mass transfer limiting current density, as shown below:

$$\frac{1}{i_{c(O_2)}} = \frac{1}{i_{\alpha(O_2)}} + \frac{1}{i^d_{\lim(O_2)}} \tag{60}$$

The charge transfer current density of this reaction is given by:

$$i_{\alpha(O_2)} = i_{o(O_2)} \cdot 10^{-\frac{E_{corr} - E_{rev(O_2)}}{b_{c(O_2)}}} \tag{61}$$

The exchange current density of oxygen reduction is a function of temperature, and can be calculated from:

$$i_{o(O_2)} = i^{ref}_{o(O_2)} \cdot e^{\frac{-\Delta H_{O_2}}{R}\left(\frac{1}{T_c + 273.15} - \frac{1}{T_{c,ref} + 273.15}\right)} \tag{62}$$

The reversible potential of this reaction does not change significantly within the range of temperature and pH of interest. Therefore, it is taken to be a constant at 0.5V.

The Tafel slope of this reaction is given by:

$$b_{c_{(O_2)}} = \frac{2.303\,R\left(T_c + 273.15\right)}{F} \tag{63}$$

The mass transfer limiting current density $i^{d}_{\lim(O_2)}$ can be obtained from

$$i^{d}_{\lim,O_2} = 4\,k_{m(O_2)}\,F\,c_{O_2} \tag{64}$$

Again, mass transfer coefficient of oxygen can be obtained in the similar fashion as described for other species.

It is worthy of mentioning here that due to the high reversible potential of oxygen reduction, this reaction is almost always under mass transfer control in the potential region of interest.

2.2.6 Reduction of water

Since water molecules are present in virtually unlimited quantities at the steel surface, it can be assumed that the reduction rate of H_2O is controlled by the charge-transfer process and, hence, pure Tafel behavior:

$$i_{c(H_2O)} = i_{o(H_2O)} \cdot 10^{-\frac{E_{corr} - E_{rev(H_2O)}}{b_{c(H_2O)}}} \tag{65}$$

Since the reduction of H_2O and H^+ are equivalent thermodynamically, they have the same reversible potential at a given pH:

$$E_{rev(H_2O)} = -\frac{2.303\ R\left(T_c + 273.15\right)}{F}\, pH \tag{66}$$

The exchange current density for water reduction $i_{o(H_2O)}$ depends on temperature:

$$\frac{i_{o(H_2O)}}{i_{o(H_2O)}^{ref}} = e^{-\frac{\Delta H_{(H_2O)}}{R}\left(\frac{1}{T_c + 273.15} - \frac{1}{T_{c,\,ref} + 273.15}\right)} \tag{67}$$

The Tafel slope for H_2O reduction was found to be the same as that for H^+ reduction:

$$b_{c(H_2O)} = \frac{2.303\ R\left(T_c + 273.15\right)}{0.5\ F} \tag{68}$$

2.3 Transport Processes in CO_2 Corrosion of Mild Steel

From the description of the electrochemical processes above it is clear that certain species in the solution are "produced" at the metal surface (e.g. Fe^{2+}) while others are depleted (e.g. H^+). The established concentration gradients lead to molecular diffusion of the species towards and away from the surface. In cases when the diffusion processes are much faster than the electrochemical processes, the

concentration change at the metal surface is small. Vice versa, when the diffusion is unable to "keep up" with the rate of the electrochemical reactions, the concentration of species at the metal surface can become very different from the ones in the bulk solution. On the other hand, the rate of the electrochemical processes depends on the species concentrations at the surface. Therefore there exists a two-way coupling between the electrochemical processes at the metal surface (corrosion) and processes in the adjacent solution layer (i.e. diffusion in the boundary layer). The same is true for chemical reactions which interact with both the transport and electrochemical processes in a complex way.

In most practical systems the water solution moves with respect to the metal surface. Therefore, the effect of convection on transport processes cannot be ignored. Turbulent eddies can penetrate deep into the hydrodynamic boundary layer and significantly alter the rate of species transport to and from the surface. Very close to the surface no turbulence can exist and the species are transported solely by diffusion. The effect of turbulent flow is captured easiest by using the concept of mass transfer coefficient, described below.

In turbulent flow of dilute ideal solutions, a mass transfer coefficient k_m for a given species (H^+, H_2CO_3, HAc, O_2 etc.) can be calculated from a correlation, such as straight pipe correlation of Berger and Hau:[25]

$$Sh_p = 0.0165 \cdot Re^{0.86} \cdot Sc^{0.33} \qquad (69)$$

or a rotating cylinder correlation of Eisenberg et al.:[26]

$$Sh_r = 0.0791 \cdot Re^{0.7} \cdot Sc^{0.356} \quad (70)$$

or any other similar correlation for the flow geometry at hand. It should be noted that most of the mass transfer correlations found in the literature (including the two listed above) are suited only for single-phase flow. Therefore, extension of this approach to multiphase flow situations needs to be done with careful consideration.

Overall, CO_2 corrosion of mild steel is not very sensitive to flow, at least not so when compared to mild steel corrosion in strong acids. This is due to the fact that the main corrosive species in CO_2 corrosion is H_2CO_3, which can easily be depleted due to a slow chemical step which precedes it: the hydration reaction (6). Therefore the limiting rate of CO_2 corrosion is primarily affected by the rate of this chemical reaction (47) which is a function of temperature and CO_2 partial pressure and not very sensitive to flow. On the other hand, HAc corrosion is primarily limited by how fast one can transport HAc to the steel surface. In contrast with CO_2 corrosion, there is no slow chemical step in HAc corrosion which precedes it and is rate limiting. Therefore flow strongly affects the limiting rate of the cathodic reaction due the presence of organic acids, and plays a more significant role in the overall corrosion process.

Clearly there is a parallel argument between CO_2 and HAc corrosion which stems in both cases from the fact that one finds a weak acid in the aqueous phase, which gives rise to higher corrosion rates than would be expected from looking at the pH alone. The main difference arises from the phase behaviour of the two solutions. In the

temperature range of interest, HAc can be found primarily in the aqueous phase and therefore its behaviour is not significantly affected by the presence of the HAc vapor. With CO_2 it is the opposite, i.e. the gaseous CO_2 controls the amount of CO_2 dissolved and the amount of H_2CO_3 found in the solution. Therefore CO_2 corrosion is significantly affected by the presence of the gaseous phase.

2.4 Calculation of Mild Steel CO_2 Corrosion Rate

Once the speciation of the aqueous CO_2 solution (including the pH, H_2CO_3 concentration, etc.) is resolved, using the thermodynamic approach outlined in section 2.1, the corrosion rate of mild steel can be calculated by using the electrochemical theory outlined in section 2.2. The unknown corrosion potential E_{corr} in (30), (34), (41), (55), (61) and (65) and can be found from the current (charge) balance equation at the steel surface:

$$i_{c(H^+)} + i_{c(H_2CO_3)} + i_{c(HAc)} + i_{c(O_2)} + i_{c(H_2O)} = i_{a(Fe)} \qquad (71)$$

When the calculated value of E_{corr} is now returned to (30), (34), (41), (55), (61) and (65), the rate of each individual reaction can be computed. This includes the so called "corrosion current density" obtained from (30):

$$i_{corr} = i_{a(Fe)} \qquad (72)$$

Finally the so called CO_2 corrosion rate is then recovered by using Faraday's law:

$$CR = \frac{i_{corr} M_{Fe}}{\rho_{Fe} nF} \tag{73}$$

If the unit A/m^2 is used for the corrosion current density i_{corr}, then conveniently the corrosion rate for iron and steel expressed in mm/y takes almost the same numerical value, precisely: $CR = 1.155\, i_{corr}$.

2.5 Successes and limitations of modeling of aqueous CO_2 corrosion of mild steel

Evidence that our basic understanding of the processes underlying CO_2 corrosion of mild steel is reasonably sound can be found by comparing the predictions made by the mechanistic model outlined above with experimental values. In Figure 2 below one can see the comparison of a potentiodynamic sweep obtained in the experiments and the one predicted by the model. Many other comparisons of the predicted and measured corrosion rates are given in the following section where the effect of key factors in CO_2 corrosion of mild steel is discussed.

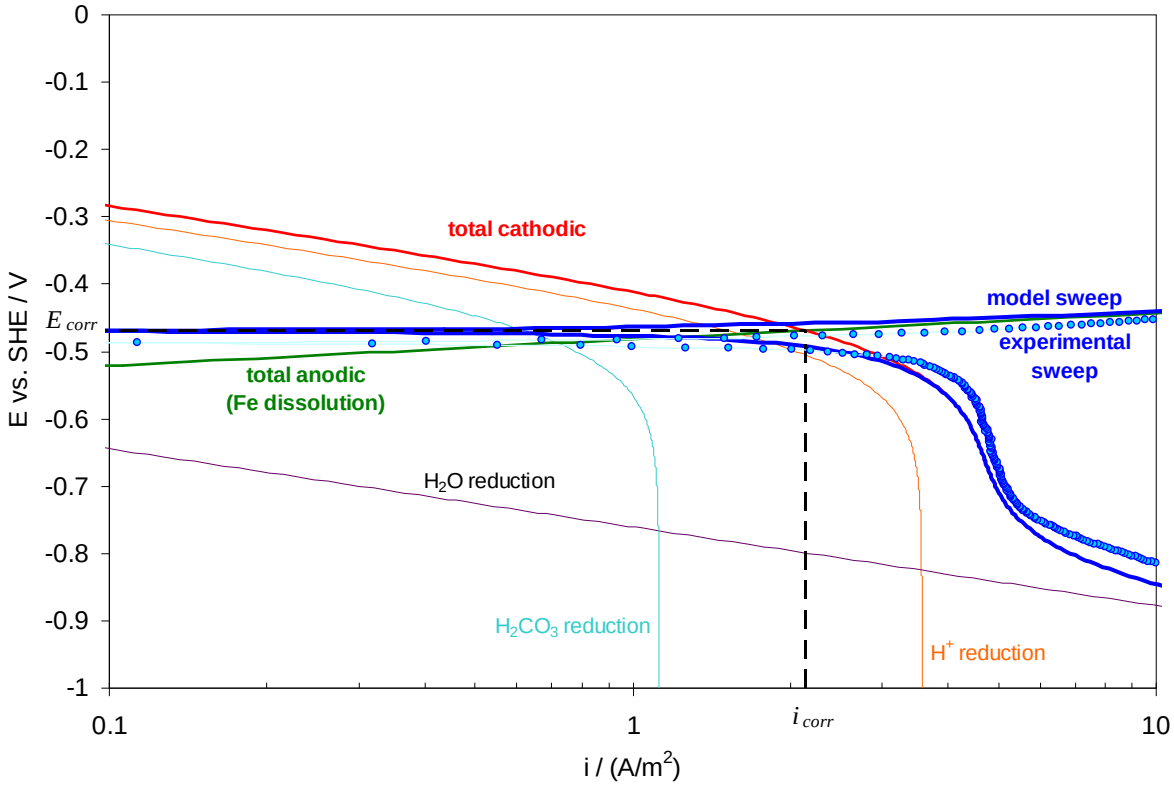

Figure 2. Potentiodynamic sweep, experimental vs. model; 20°C, p_{CO_2} =1 bar, pH4, 2 m/s.

Regardless the relative progress we have made in understanding and modeling of aqueous CO_2 corrosion of mild steel, many questions persist. One is the issue of localized CO_2 corrosion which is still a topic of intense ongoing research. Effect of other factors such as steel metallurgy, organic acids, oxygen, multiphase flow and inhibitors are challenges that need further effort. Some of those are discussed in the following sections.

2.6 Key Factors Affecting Aqueous CO_2 Corrosion of Mild Steel

2.6.1 The effect of pH

pH has a strong influence on the corrosion rate. Typical pH in CO_2 saturated condensed water is about pH 4 while in buffered brines, one frequently encounters 5<pH<7. At pH 4 or below, direct reduction of H^+ ions, reaction (23), is important particularly at lower partial pressure of CO_2 when the pH has a direct effect on the corrosion rate. However, the most important effect of pH is indirect and relates to how pH changes conditions for formation of ferrous carbonate layers. High pH results in a decreased solubility of ferrous carbonate and leads to an increased precipitation rate and a higher scaling tendency. The effect of various pH and supersaturations are shown in Figure 3. At lower supersaturations obtained at the lower pH6, the corrosion rate does not change much with time, even if some ferrous carbonate precipitation occurs, reflecting the fact that a relatively porous, detached and unprotective layer is formed (low scaling tendency ST). The higher pH6.6 results in higher supersaturation, faster precipitation and formation of more protective ferrous carbonate, reflected by a rapid decrease of the corrosion rate with time. There are other indirect effects of pH, and by almost all accounts, higher pH leads to a reduction of the corrosion rate, making the "pH stabilization" (meaning: pH increase) technique an attractive way of managing CO_2 corrosion. The drawback of this technique is that it can lead to excessive scaling and can be rarely used with formation water systems.

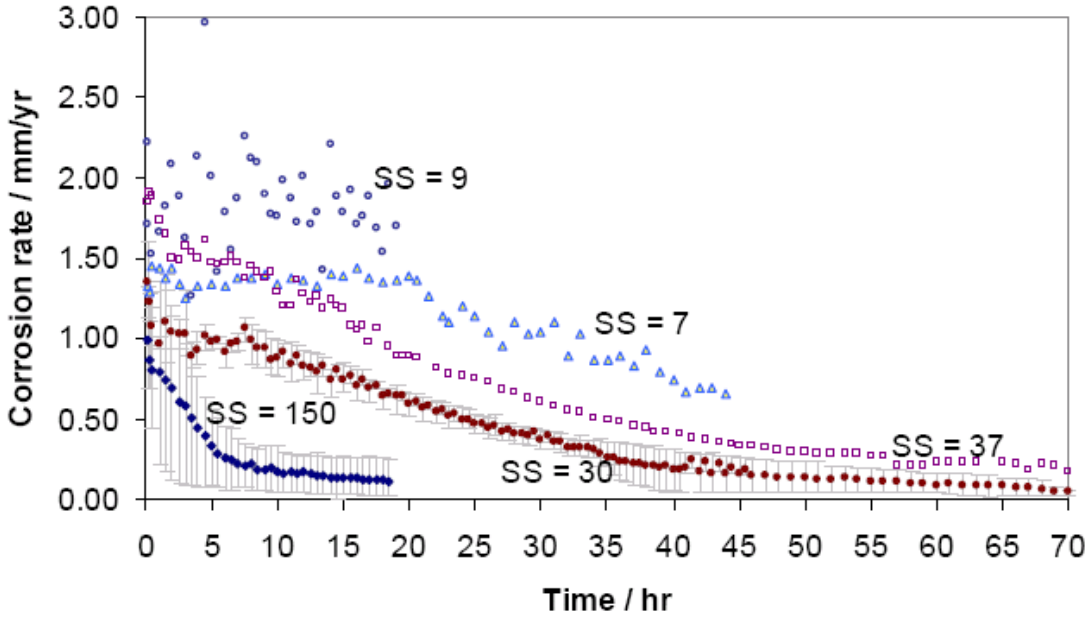

Figure 3. Effect of ferrous carbonate supersaturation $SS_{(FeCO_3)}$ on corrosion rate obtained at a range of pH6.0-pH6.6, for 5 ppm< $c_{Fe^{2+}}$ < 50 ppm at T = 80°C, under stagnant conditions. Error bars represent minimum and maximum values obtained in repeated experiments. Data taken from Chokshi et al. [17]

2.6.2 The effect of CO_2 partial pressure

In the case of scale-free CO_2 corrosion, an increase of p_{CO_2}, typically leads to an increase in the corrosion rate. The commonly accepted explanation is that with p_{CO_2} the concentration of H_2CO_3 increases and accelerates the cathodic reaction, equation (25), and ultimately the corrosion rate. The detrimental effect of p_{CO_2} at a constant pH is illustrated in Figure 4. The model described above reasonably well captures this trend up to approximately p_{CO_2} =10 bar.

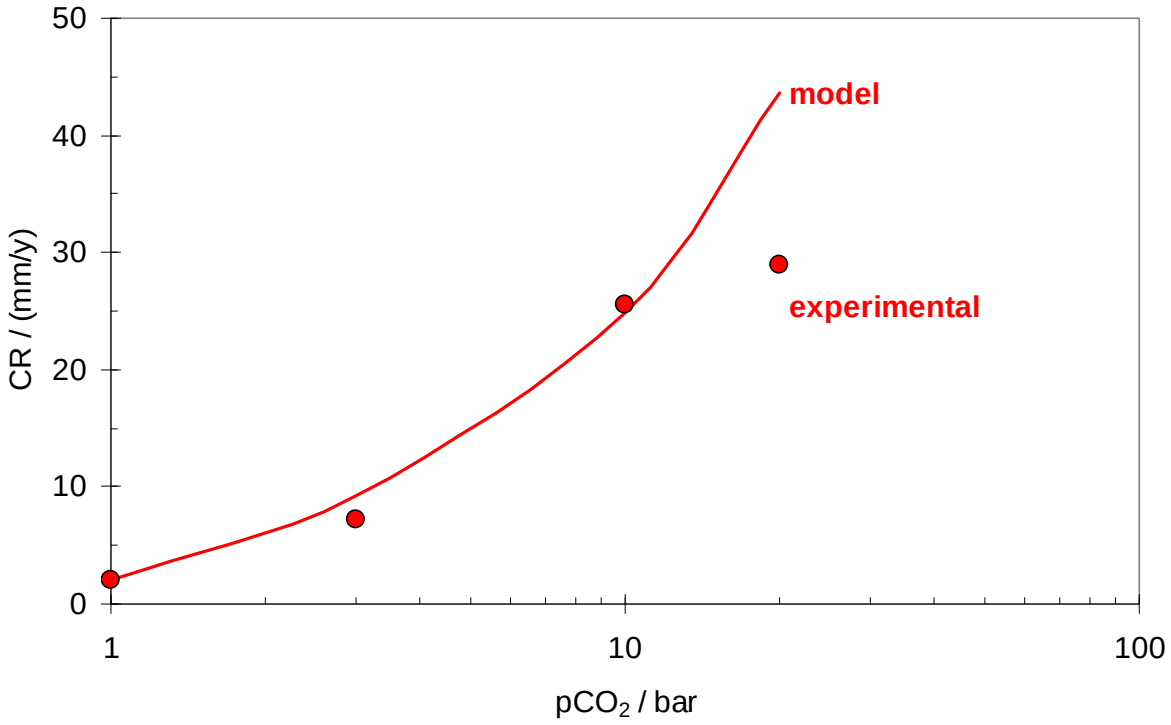

Figure 4. The effect of CO_2 partial pressure, p_{CO_2} on bare steel corrosion rate, comparison of experimental results and model; 60°C, pH5, 1 m/s, 100 mm ID single-phase pipe flow.

However, when other conditions are favorable for formation of ferrous carbonate layers, increased P_{CO_2} can have a beneficial effect. At a high pH, higher P_{CO_2} leads to an increase in bicarbonate and carbonate ion concentration and a higher supersaturation, which accelerates precipitation and protective layer formation. The effect of P_{CO_2} on the corrosion rate in the presence of ferrous carbonate precipitation is illustrated in Figure 5 where in stratified wet gas flow, corrosion rate is reduced both at top and bottom of the pipe with the increase partial pressure of CO_2.

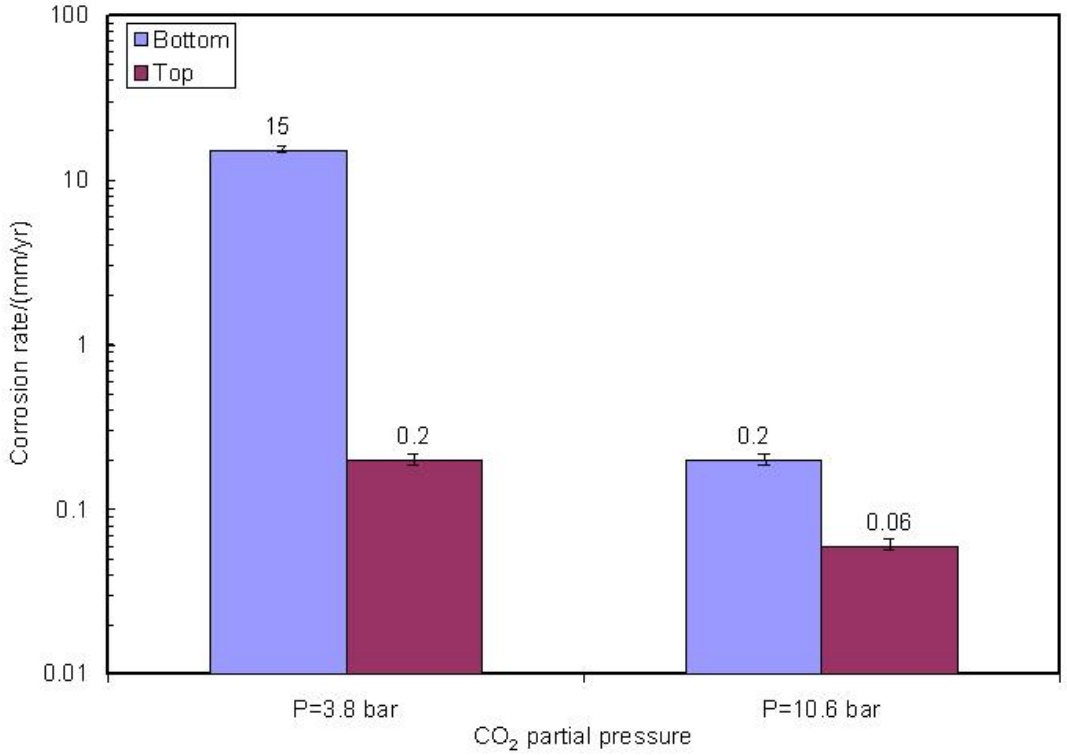

Figure 5. Experimental measurements of the corrosion rate at the top and bottom of the pipe in stratified gas-liquid flow showing the effect of CO_2 partial pressure, p_{CO_2} on formation of ferrous carbonate layer. Test conditions: 90°C, pH6, 100 mm ID, Vsg=10 m/s, Vsl=0.1 m/s,. Data taken from Sun and Nešić[18].

2.6.3 The effect of temperature

Temperature accelerates all the processes involved in corrosion: electrochemical, chemical, transport, etc. One would expect then that the corrosion rate steadily increases with temperature, and this is the case at low pH when precipitation of ferrous carbonate or other protective layers does not occur. An example is shown in Figure 6. The situation changes markedly when solubility of ferrous carbonate is exceeded, typically at a higher pH. In that case, increased temperature accelerates rapidly the kinetics of precipitation and protective layer formation, decreasing the

corrosion rate. The peak in the corrosion rate is usually seen between 60°C and 80°C depending on water chemistry and flow conditions. Many of empirical models are built to mimic this behavior without accounting for the complication effect of pH. as shown in Figure 6(dotted line).

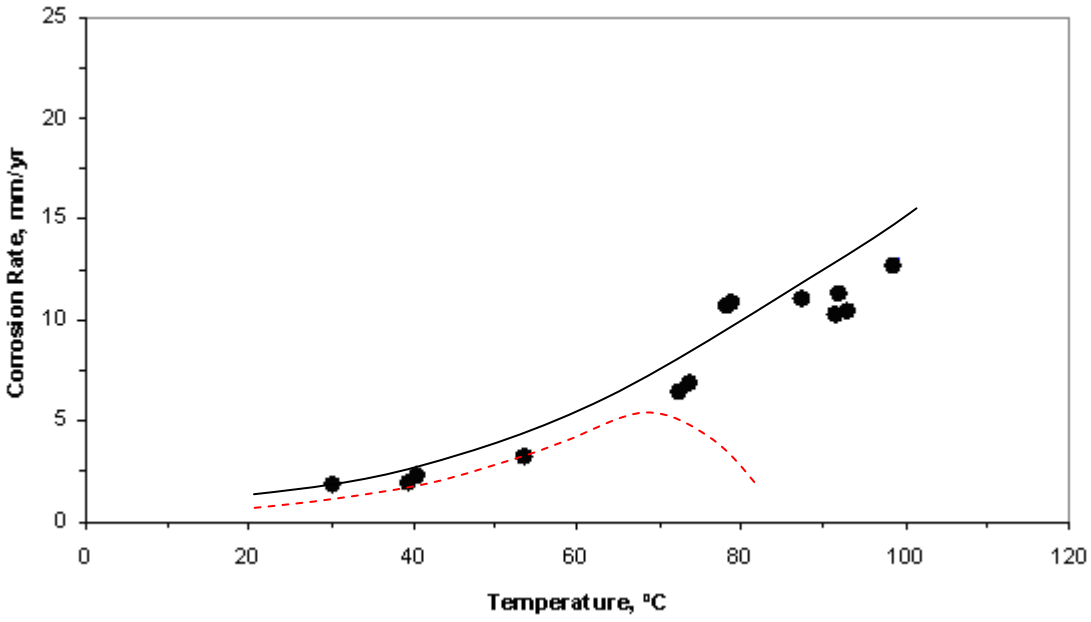

Figure 6. The effect of temperature on CO_2 corrosion rate of mild steel; pH 4, P_{CO_2} = 1bar, 100 mm ID single phase pipe flow. Points are experimental values and the solid line is the model. The red dotted line is a model simulation of the same conditions at pH6.6.

2.6.4 The effect of flow

There are two main ways in which flow may affect CO_2 corrosion which can be distinguished based on whether or not other conditions are conducive to protective layer formation or not.

In the case of corrosion where protective layers do not form (typically at low pH as found in condensed water and in the absence of inhibitors), the main role of turbulent flow is to enhance transport of species towards and away from the metal surface. This may lead to an increase in the corrosion rate as illustrated in Figure 7. At lower pH4, the effect is much more pronounced as the dominant cathodic reaction is direct H^+ ion reduction (23), which is under mass transfer control (see Equation (39)).

When protective ferrous carbonate layers form (typically at higher pH in produced water) or when inhibitor films are present on the steel surface, the above-mentioned effect of flow becomes insignificant as the main resistance to corrosion is now in the surface layer or inhibitor film. In this case, the effect of flow is to interfere with formation of protective surface layers or to remove them once they are in place, often leading to an increased risk of localized attack.

The two flow accelerated corrosion effects discussed above are frequently aggravated by flow disturbances such as valves, constrictions, expansions, bends, etc. where local increases of near-wall turbulence and wall-shear stress are seen. However, flow can lead to onset of localized attack only when given the "right" set of circumstances as discussed in a separate heading below.

The effect of multiphase flow on CO_2 corrosion is complicated by the different flow patterns that exist, most common being: *stratified*, *slug* and *annular-mist* flow. In the liquid phase, water and oil can flow separated or mixed with either phase being continuous with the other flowing as a dispersed phase. Different flow patterns lead to a variety of steel surface wetting mechanisms: stable water wetting, stable oil wetting, intermittent wetting, etc., which greatly affect corrosion. In annular mist flow,

the liquid droplets move at high velocity and can may lead to protective layer damage at points of impact such as bends, valves, tees, constrictions/expansions and other pipe fitting. Slug flow can lead to significant short lived fluctuations in the wall-shear stress which can help remove a protective surface layer of ferrous carbonate or affect an inhibitor film.

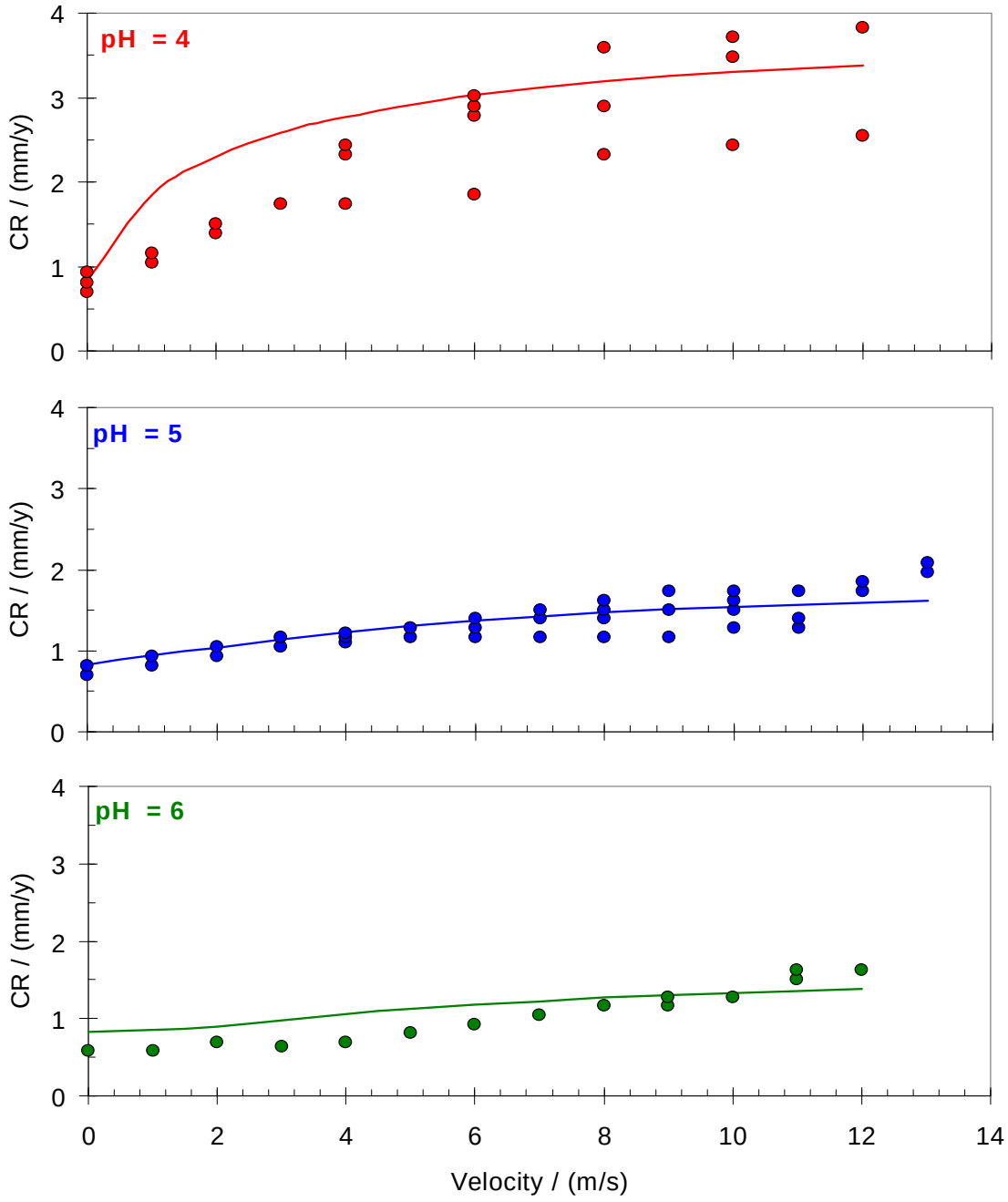

Figure 7. Predicted and experimentally measured corrosion rates showing the effect of velocity in the absence of ferrous carbonate layers. Test conditions: 20°C, p_{CO_2} = 1 bar, 15 mm ID single-phase pipe flow. Experimental data taken from Nešić et al.[19]

2.6.5 Effect of corrosion inhibition

The two most common sources of corrosion inhibition need to be considered:

a) inhibition by addition of corrosion inhibitors and

b) inhibition by components present in the crude oil.

a) Corrosion inhibitors

Describing the effect of corrosion inhibitors is not a straightforward task due to the enormous complexity of the subject. Quantifying them and predicting their behavior is even harder. There is a plethora of approaches in the open literature, varying from the use of simple *inhibitor factors* and *inhibition efficiencies* to the application of complicated *molecular modeling* techniques to describe inhibitor interactions with the steel surface and ferrous carbonate layer. A middle-of-the-road approach is based on the assumption that corrosion protection is achieved by *surface coverage*, i.e. that the inhibitor adsorbs onto the steel surface and slows down one or more electrochemical reactions by "blocking". The degree of protection is assumed to be directly proportional to the fraction of the steel surface blocked by the inhibitor. In this type of model one needs to establish a relationship between the surface coverage θ and the inhibitor concentration in the solution c_{inh}. This is most commonly done by the use of adsorption isotherms.

b) Corrosion inhibition by crude oil

It has been known for a while that CO_2 corrosion rates seen in the field in the presence of crude oil are much lower then those obtained in laboratory conditions where crude

oil was not used or synthetic crude oil was used. One can identify two main effects of crude oil on the CO_2 corrosion rate.

The first is a *wettability* effect and relates to a hydrodynamic condition where crude oil entrains the water and prevents it from wetting the steel surface (continuously or intermittently).

The second effect is *corrosion inhibition* by components of the crude oil that reach the steel surface either by direct contact or by first partitioning into the water phase. Various surface active organic compounds found in crude oil (typically oxygen, sulfur and nitrogen containing molecules) have been identified to directly inhibit corrosion of mild steel in CO_2 solutions.

2.6.6 The effect of organic acids

The effect of HAc is particularly pronounced at higher temperatures and low pH when the abundance of undissociated HAc can increase the CO_2 corrosion rate dramatically as seen in Figure 8. Solid iron acetate does not precipitate in the pH range of interest since iron acetate's solubility much higher than that of ferrous carbonate. There are some indications that the presence of organic acids impairs the protectiveness of ferrous carbonate layers, however the mechanism is still not clear.

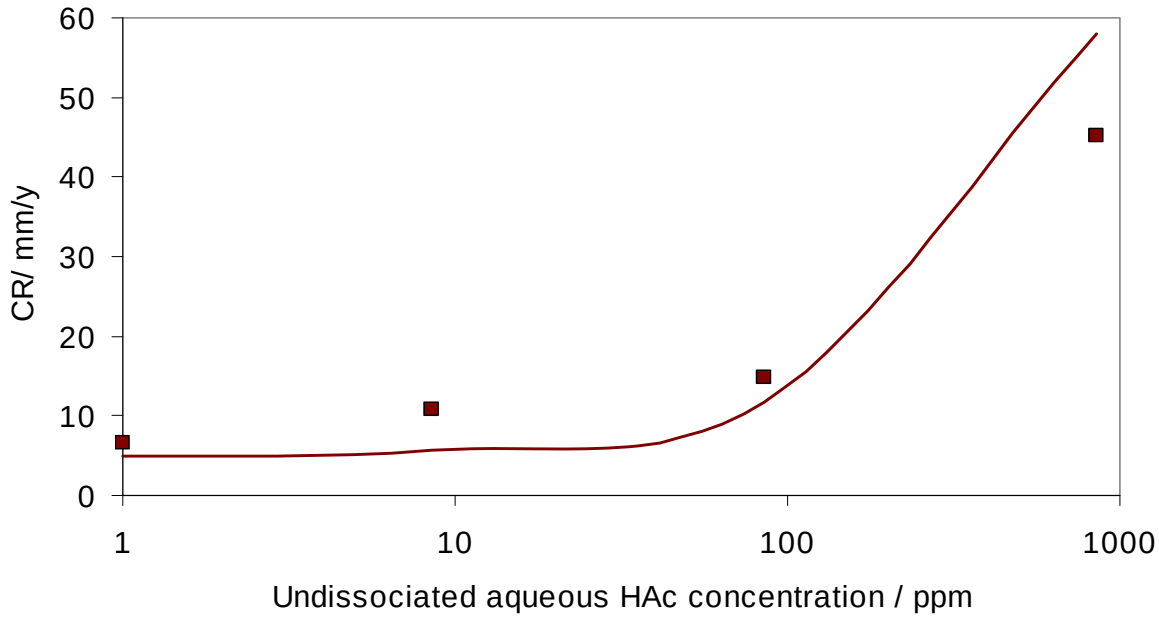

Figure 8. The effect of the concentration of undissociated acetic acid (HAc) on the CO_2 corrosion rate, 60°C, p_{CO_2} =0.8 bar, pH4, 12 mm OD rotating cylinder flow at 1000 rpm. Experimental data taken from Geroge and Nešić et al.[20]

2.6.7 Effect of glycol/methanol

Glycol and methanol are often added to flowing systems in order to prevent hydrates from forming. The quantities are often significant (50% of total liquid phase is not unusual). In the very few studies available it has been assumed that the main "inhibitive" effect of glycol/methanol on corrosion comes from dilution of the water phase, which leads to a decreased activity of water. However, there are many unanswered questions such as the changes in mechanisms of CO_2 corrosion in water/glycol mixtures which have yet to be discovered.

2.6.8 Effect of condensation in wet gas flow

When transporting humid natural gas, due to the cooling of the stream, condensation of water vapor occurs on the internal pipe wall. The condensed water is pure and, due to dissolved CO_2 , has typically a pH<4. This leads to the so-called *top-of-the-line corrosion* (TLC) scenario. If the rate of condensation is high, plenty of acidic water flows down the internal pipe walls leading to a very corrosive situation. If the condensation rate is low, the water film is not renewed and flows down very slowly and the corrosion process can release enough Fe^{2+} to raise the local pH and saturate the solution, leading to formation of protective ferrous carbonate layer. The layer is often protective, however incidents of localized attack in TLC were reported.[21] Either way, the stratified or stratified-wavy flow regime, typical for TLC, does not lead to a good opportunity for inhibitors to reach the upper portion of the internal pipe wall and protect it. A very limited range of corrosion management options for TLC exists. To qualitatively and quantitatively describe the phenomenon of corrosion occurring at the top of the line, a deep insight into the combined effect of the chemistry, hydrodynamics, thermodynamics, and heat and mass transfer in the condensed water is needed. A full description exceeds the scope of this review, and the interested reader is directed to see some recent articles published on this topic.[21, 22]

2.6.9 Non-ideal solutions and gases

In many cases produced water has a very high dissolved solids content (>10 wt%). At such high concentrations, the infinite dilution theory used above does not hold and corrections need to be made to account for solution non-ideality. A simple way to account for the effect on non-ideal homogenous water chemistry is to correct the

equilibrium constants by using the concept of ionic strength as indicated above. This approach seems to work well only for moderately concentrated solution (up to a few wt% of dissolved solids). For more concentrated solutions a more accurate way is to use activity coefficients as described by Anderko et al.[23] The effect of concentrated solutions on heterogeneous reactions such as precipitation of ferrous carbonate and other layers is still largely unknown. Furthermore, it is unclear how the highly concentrated solutions affect surface electrochemistry. Some experience suggests that corrosion rates can be dramatically reduced in very concentrated brines, nevertheless a more systematic study is needed.

At very high total pressure the gas/liquid equilibria cannot be accounted for by Henry's law. A simple correction can be made by using a fugacity coefficient which accounts for non-ideality of the CO_2/natural gas mixture[24] and can be obtained by solving the equation of state for the gas mixture.

2.7 Localized CO_2 Corrosion of Mild Steel in Aqueous Solutions

As illustrated above, significant progress has been achieved in understanding uniform CO_2 corrosion, without or with protective layers, and hence a successful uniform corrosion models can be built. However, much less is known about localized CO_2 corrosion. It is thought that one of the main factors that "triggers" localized attack is flow, tempered by other environmental variables such as pH, temperature, partial pressure of CO_2, etc. It seems that localized attack occurs when the conditions are such that partially protective ferrous carbonate layer form. It is well known that when

fully protective ferrous carbonate forms – low general corrosion rates are obtained and vice versa: when no protective layers form – a high rate of general corrosion is seen. It is when the corrosive environment is "in between", in the so called "grey zone", that localized attack can be initiated most often by some extreme flow conditions. There are many combinations of environmental and metallurgical parameters that define the grey zone, making this sound like a difficult proposal. However, there is a single parameter which is easy to calculate: ferrous carbonate supersaturation, $SS_{(FeCO_3)}$ (see Equation (18) above), which can be successfully used as a good delineator for the grey zone and as such as a predictor for the probability for localized attack. When bulk ferrous carbonate supersaturation in the range $0.5 < SS_{(FeCO_3)} < 2$ there is a risk of localized attack. The further away the solution is from these boundaries, the lower the risk. The scaling tendency ST (see Equation (21) above) is conceptually even better suited as a predictor of localized corrosion risk, however its calculation is much more difficult and uncertain as it involves calculation of both the uniform corrosion rate and the precipitation rate.

Based on mostly anecdotal evidence (field experience), the presence of H_2S and HAc was related to onset of localized attack, however little is understood about how and when this may happen.

3 AQUEOUS H_2S CORROSION OF MILD STEEL

Internal corrosion of mild steel in the presence of hydrogen sulfide (H_2S) also represents a significant problem for the oil and gas industry[27-33]. Increasingly more fields are being developed that in addition to CO_2 have high concentrations of H_2S.

In CO_2/H_2S corrosion of mild steel, both ferrous carbonate and ferrous sulfide layers can form on the steel surface. Studies have demonstrated that sulfide layer formation is one of the important factors governing the H_2S corrosion rate. The sulfide layer growth depends primarily on the kinetics of the corrosion process as is described below.

Despite the relative abundance of experimental data on H_2S corrosion of steel, most of the literature is still confusing and somewhat contradictory. Therefore the mechanism of H_2S corrosion remains much less understood when compared to that of CO_2 corrosion. This uncertainty makes it more difficult to develop a model to predict the corrosion rate of mild steel in H_2S saturated aqueous solution.

3.1 Chemistry of H_2S Saturated Aqueous Solutions – Equilibrium Considerations

Similarly to CO_2 discussed above, the H_2S gas is also soluble in water:

$$H_2S_{(g)} \overset{K_{H_2S}}{\Leftrightarrow} H_2S \tag{74}$$

where K_{H_2S} is the solubility constant of H_2S in mol/(l bar):

$$K_{sol(H_2S)} = \frac{c_{H_2S}}{p_{H_2S}} \tag{75}$$

and can be found from:[34]

$$K_{sol(H_2S)} = 10^{-\left(634.27+0.2709T_K-0.11132*10^{-3}T_K^2-\frac{16719}{T_K}-261.9\log T_K\right)} \quad (76)$$

As shown in Figure 9, the solubility of H_2S decrease with temperature, the same as is observed for CO_2. However, for the same partial pressure and temperature, the concentration of dissolved H_2S actually exceeds that in the gas phase as shown in Figure 10.

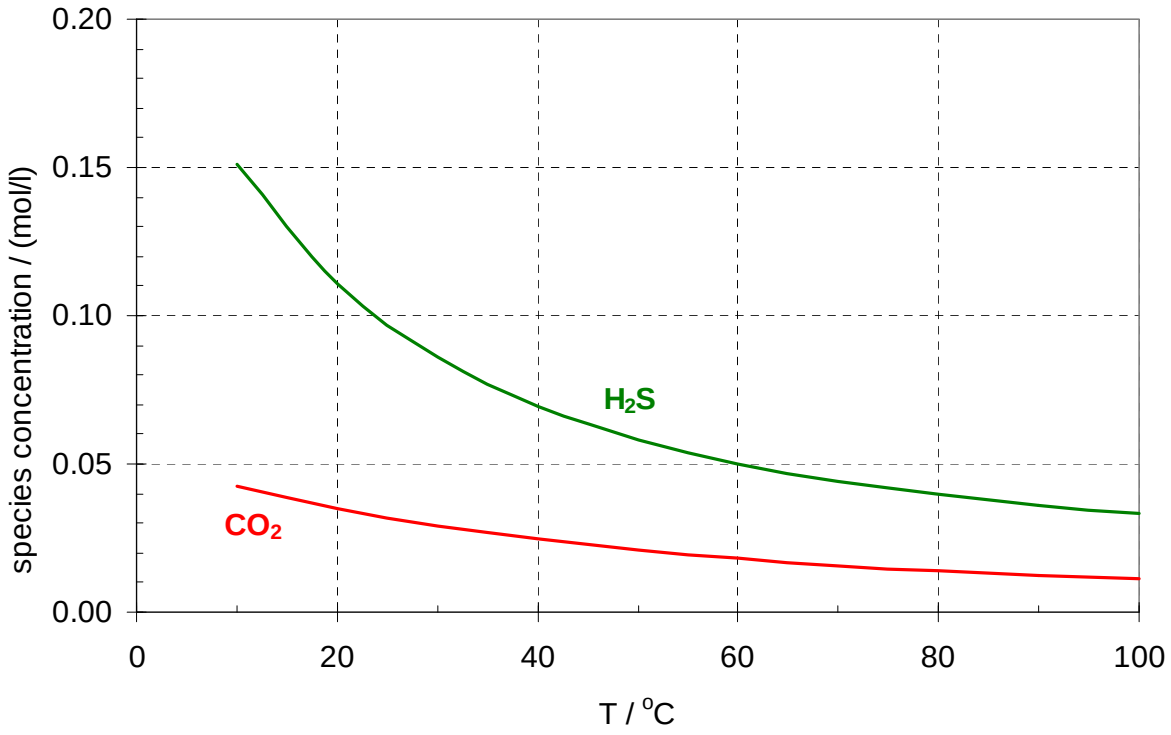

Figure 9. Solubility of H_2S and CO_2 as a function of temperature; 25°C, p_{H_2S}=1 bar, p_{CO_2}=1 bar.

The aqueous H_2S is another weak acid which partly dissociates in two steps:

$$H_2S \overset{K_{hs}}{\Leftrightarrow} H^+ + HS^- \quad (77)$$

$$HS^- \overset{K_{bs}}{\Leftrightarrow} H^+ + S^{2-} \tag{78}$$

where K_{hs} is the dissociation constant of H_2S:

$$K_{hs} = \frac{c_{H^+} c_{HS^-}}{c_{H_2S}} \tag{79}$$

and can be calculated as:[35]

$$K_{hs} = 10^{-(15.345 - 0.045676\, T_K + 5.9666 \times 10^{-5}\, T_K^2)} \tag{80}$$

and K_{bs} is the dissociation constant of HS^-:

$$K_{bs} = \frac{c_{H^+} c_{S^{2-}}}{c_{HS^-}} \tag{81}$$

There is very large discrepancy in the reported values for K_{bs}, varying from 1.0×10^{-19} to 1.1×10^{-12} kmol/m^3 at room temperature (seven orders of magnitude). Hence it is suggested that the using K_{bs} to calculate the concentration of sulfide species, $c_{S^{2-}}$ and further to predict the solubility product constants for ferrous sulfides should be avoided.

Given the same gaseous concentrations of H_2S and CO_2, one obtains a similar aqueous concentration of dissolved H_2S and CO_2 (see Figure 9) and the resulting pH

is within 0.1 pH unit. The equilibrium distribution of sulfide species as a function of pH for an open system is shown in Figure 10. The concentration of bisulfide ion, c_{HS^-} becomes significant only above pH4, while the concentration of the sulfide ion, $c_{S^{2-}}$ is not even shown as it is very low and unreliable to calculate.

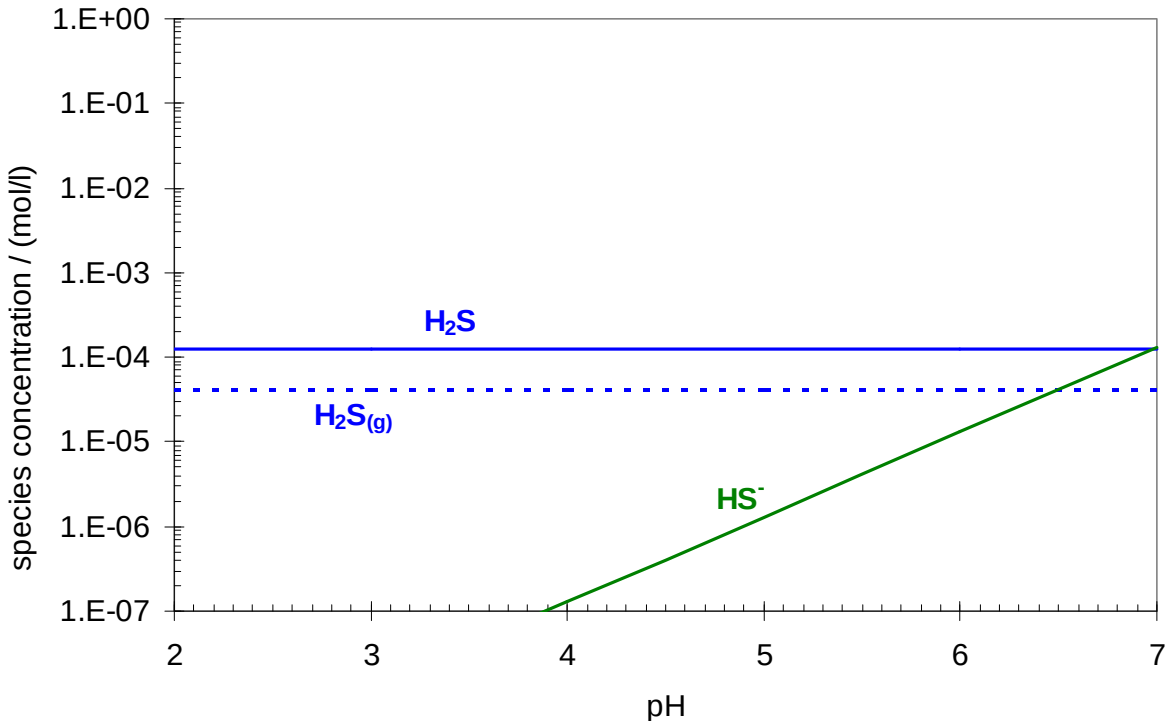

Figure 10. Sulfide species concentrations as a function of pH for a H_2S saturated aqueous solution at p_{H_2S}=1 mbar, 25°C, 1wt%NaCl.

Many types of iron sulfides occur, such as amorphous ferrous sulfide (FeS), mackinawite ($Fe_{1+x}S$), cubic ferrous sulfide (FeS), troilite (FeS), pyrrhotite ($Fe_{1-x}S$ or FeS_{1+x}), smythite ($Fe_{3+x}S_4$), greigite (Fe_3S_4) and pyrite (FeS_2). Some of these are stoichiometric such as cubic ferrous sulfide, troilite, greigite and pyrite, while others are not, such as mackinawite, pyrrhotite and smythite. The thermodynamics of these systems is very complicated; depending on environmental conditions and time,

transformation from one type of ferrous sulfide into the other occurs. Limited information exists on aqueous solubility of the various sulfides. Avoiding the usage of the sulfide ion concentration, $c_{S^{2-}}$, one can write a general equation for precipitation of ferrous sulfide as:

$$Fe^{2+} + H_2S \overset{K_{sp(FeS)}}{\Leftrightarrow} FeS_{(s)} + 2H^+ \tag{82}$$

where the solubility constant for one type of ferrous sulfide – mackinawite is known as a function of temperature:[36]

$$K_{sp(FeS)}^{mackin} = 10^{\frac{2848.779}{T_k} - 6.347} \tag{83}$$

For other ferrous sulfides only the values at room temperature are known, as listed in Table 1 below. It is convenient to show the various ferrous sulfide solubilities in terms of an equilibrium concentration of the Fe^{2+} as a function of pH at a given H_2S partial pressure (concentration). An example is presented in Figure 11 where it can be seen that the much less soluble pyrrhotite and troilite are thermodynamically more stable forms compared to mackinawite and amorphous ferrous sulfide. For a typical ferrous ion concentration of $c_{Fe^{2+}}$=1 ppm, the saturation with respect to troilite and pyrrhotite is reached already at pH5.4 while for mackinawite it is pH6 and amorphous ferrous sulfide pH6.7. Keeping in mind that the concentration of Fe^{2+} at a corroding steel surface can easily be much higher than in the bulk (e.g. 10 ppm or even higher) and that the pH is also higher at the surface than in the bulk (typically above pH6), using

Figure 11 one can expect a whole range of different ferrous sulfides to form on a corroding steel surface at this H_2S concentration at different points in time.

Images of a ferrous sulfide surface layer formed on mild steel after a week long exposure are shown in Figure 12. The layered structure of the sulfide is prominent and it can be identified as mackinawite. In longer exposures, the ferrous sulfide layer thickens and becomes eventually more protective. An image of a ferrous sulfide layer after a month long exposure is shown in Figure 13. The composition of the layer is a mixture of mackinawite and pyrrhotite. Another layered composed of a mixture of ferrous carbonate and ferrous sulfide is shown in Figure 14.

Table 1. Solubility product constants for various ferrous sulfides at 25°C.[37]

Type of ferrous sulfide	$-\log K_{sp(FeS)}$
Amorphous (FeS)	2.95
Mackinawite ($Fe_{1+x}S$)	3.6
Pyrrhotite ($Fe_{1-x}S$ or FeS_{1+x})	5.19
Troilite (FeS)	5.31

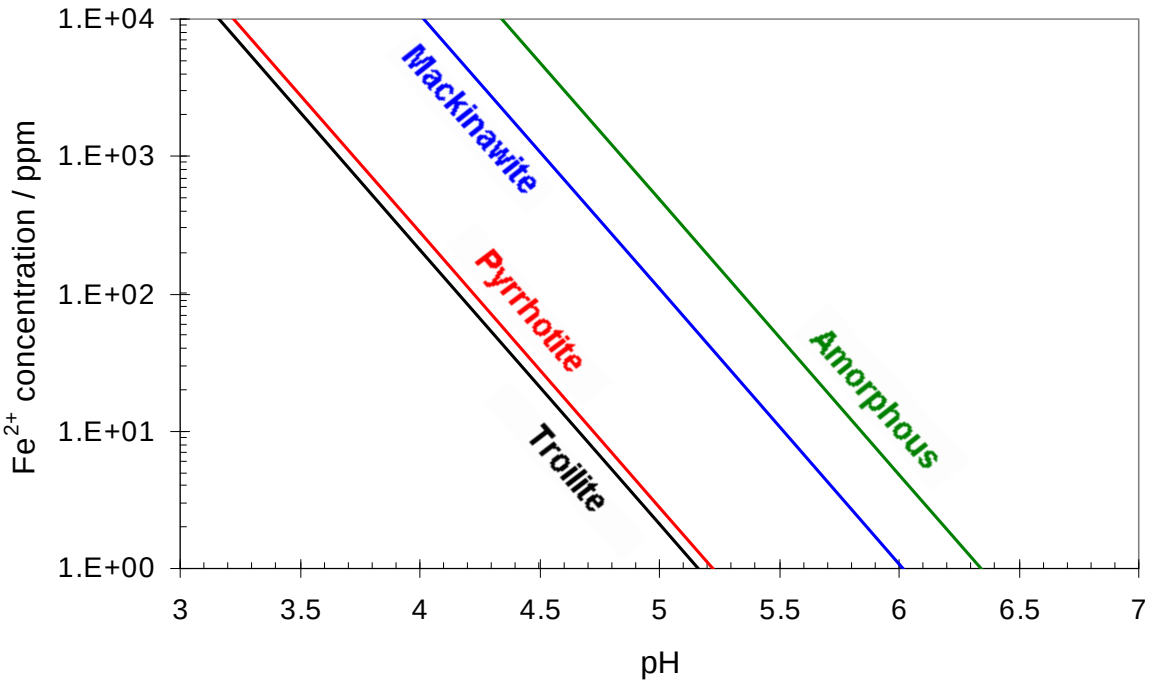

Figure 11. Solubility of various sulfides as a function of pH shown in terms of the equilibrium concentration of Fe^{2+}, p_{H_2S}=1 mbar, 25°C, 1wt%NaCl.

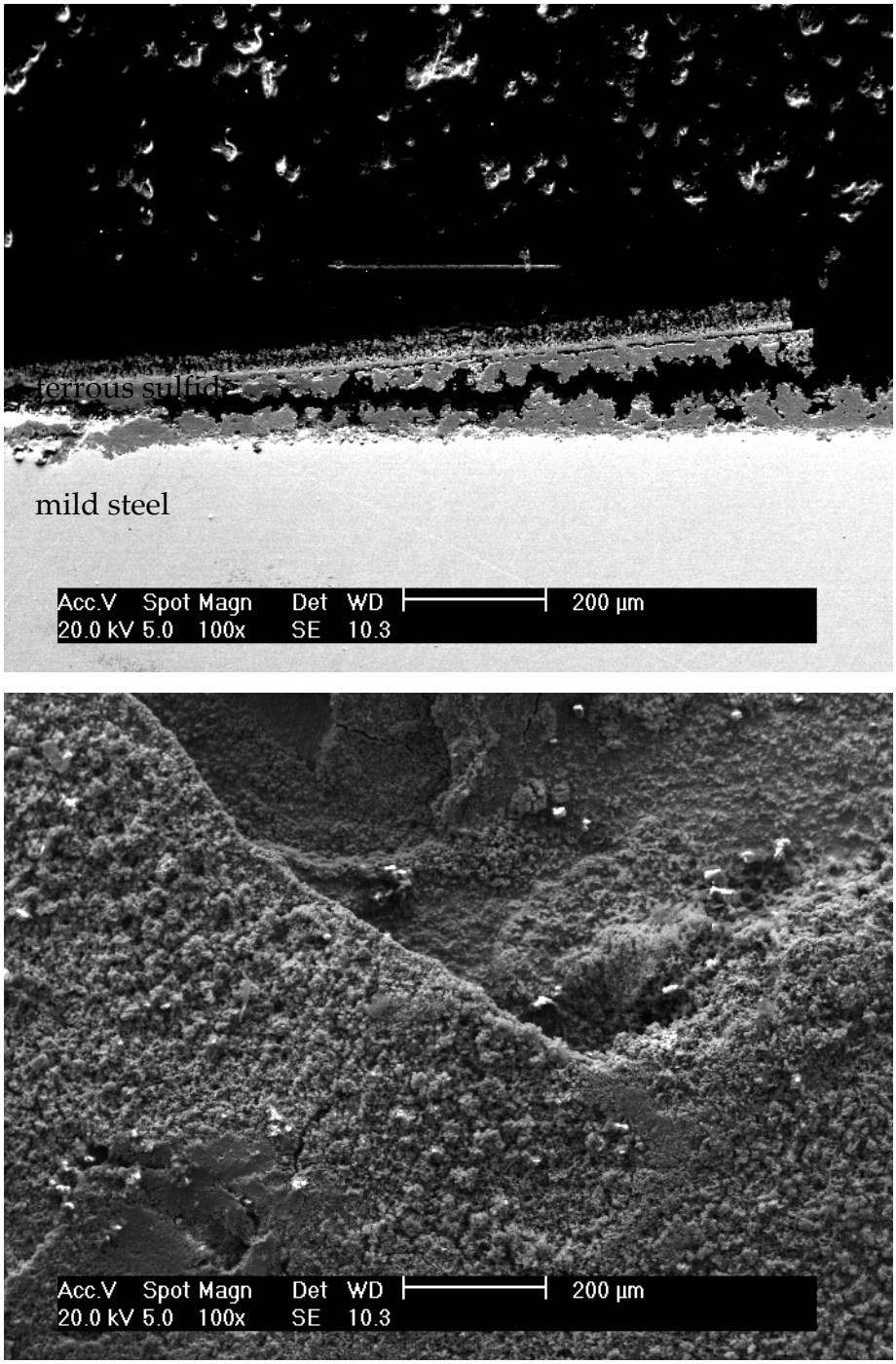

Figure 12. A cross section and a top view of a ferrous sulfide layer formed on mild steel; 60°C, pH6, p_{CO_2} =7.7 bar, p_{H_2S} =0.25 mbar, 1 m/s single phase flow in a 100 mm ID pipe, 7 days exposure.

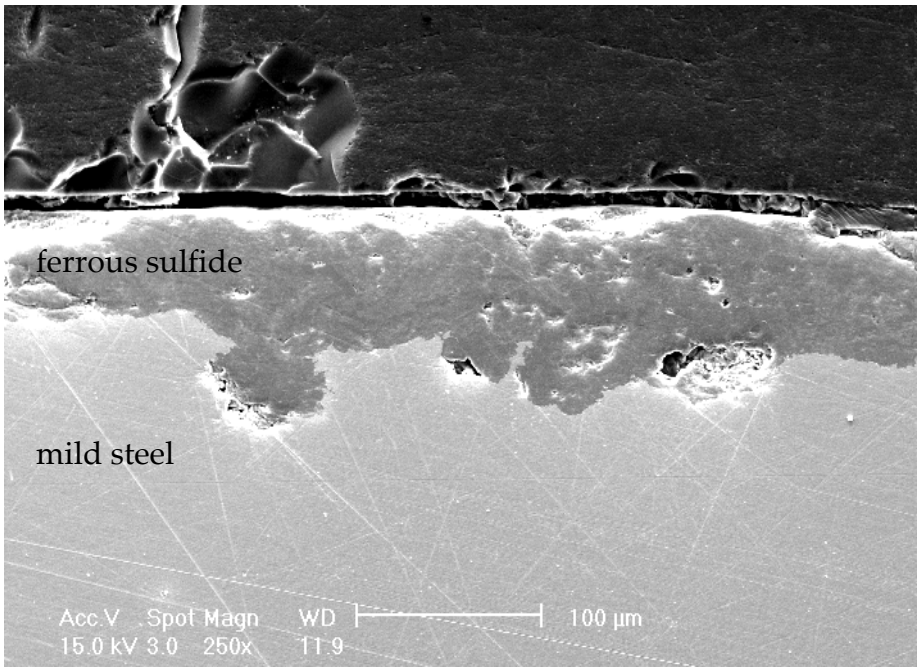

Figure 13. A cross section a ferrous sulfide layer formed on mild steel; 60°C, pH6, p_{CO_2} =7.7 bar, p_{H_2S} =0.25 mbar, 1 m/s single phase flow in a 100 mm ID pipe, 30 day exposure.

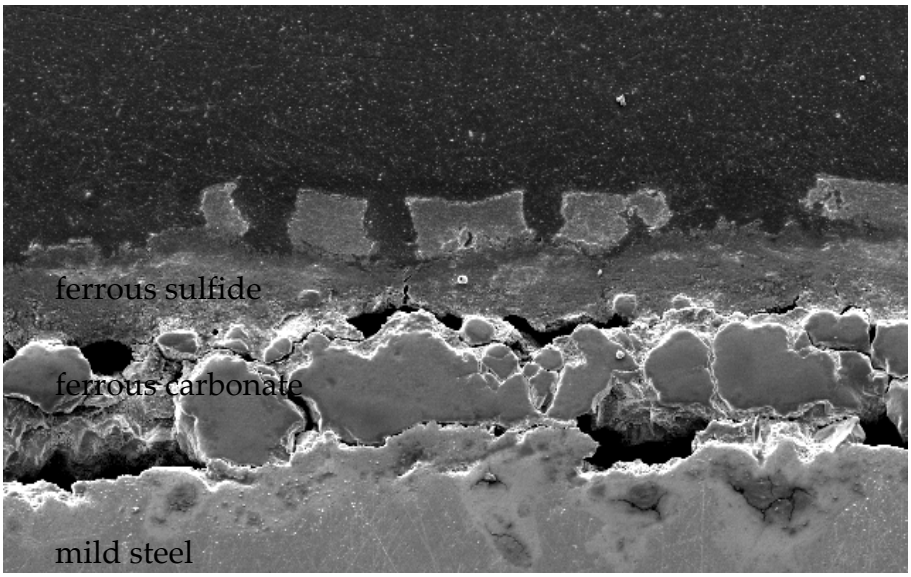

Figure 14. A cross section a mixed ferrous carbonate and ferrous sulfide layer formed on mild steel; 60°C, pH6, p_{CO_2} =7.7 bar, p_{H_2S} =1.2 mbar, 1 m/s single phase flow in a 100 mm ID pipe, 25 day exposure.

3.2 Mild Steel Corrosion in H_2S and mixed H_2S/CO_2/HAc Saturated Aqueous Solutions

As the aqueous H_2S is another weak acid, it can be seen as an additional reservoir of H^+ ions according to reaction (77), in a similar way as H_2CO_3 was discussed above. Therefore stimulation of the hydrogen evolution reaction could also be expected in the presence of H_2S. Using the analogy with CO_2 corrosion, one must also allow the possibility of direct reduction of H_2S, i.e. that the H_2S molecule can be adsorbed at the steel surface, followed by a reduction of the H^+ and oxidation of iron in the steel. As solid ferrous sulfide (mackinawite) is always found on the corroding steel surface in the presence of H_2S, one can write the corrosion reaction as:

$$Fe_{(s)} + H_2S \rightarrow FeS_{(s)} + H_2 \qquad (84)$$

This has been referred to as a "solid state" reaction pathway as both the initial and final state of *Fe* are solid (*s*).

Therefore it seems that corrosion of mild steel by H_2S initially proceeds by adsorption of H_2S to the steel surface followed by a very fast redox reaction at the steel surface to form an adherent mackinawite film (much like a tarnish). This initial mackinawite film is very thin (<<1μm) but apparently rather dense and acts as a solid state diffusion barrier for the species involved in the corrosion reaction. Therefore this thin mackinawite film is one of the most important factors governing the corrosion rate in H_2S corrosion. It also strongly affects corrosion due to CO_2.

The thin mackinawite film continuously goes through a cyclic process of growth, internal stress growth, cracking and delamination, what generates an outer sulfide layer which thickens over time (typically >>1μm) and forms an additional diffusion barrier. However, this outer sulfide layer is very porous and rather loosely attached to the steel surface, over time it may crack, peel and spall, a process aggravated by the flow.

The transformation of mackinawite into other forms of less soluble ferrous sulfide (pyrrhotite and troilite, see Figure 11) may happen over time. In addition, ferrous sulfide precipitation from the bulk is also possible. Among the various ferrous sulfides, mackinawite is the prevalent ferrous sulfide that forms in corrosion of mild steel at low H_2S concentration and low temperature. At increased levels of H_2S, mackinawite is less prevalent and pyrrhotite is the main corrosion product. At very high H_2S concentrations, pyrite and even elemental sulfur appear. While thermodynamics of ferrous sulfides may favor other types of sulfide over mackinawite as the corrosion product, the rapid kinetics of mackinawite formation favors it as the initial corrosion product seen in most situations. Overall however, there is no clear relationship between the nature of the sulfide layer and the underlying corrosion process. It is generally thought that all types of ferrous sulfide layers offer some degree of protection for mild steel.

In the presence of oxygen and at very high H_2S concentrations, elemental sulfur can appear and cause severe localized corrosion. The most likely pathway for formation of elemental sulfur is as follows:

- when there is O_2 present, some of the ferrous sulfide reacts with O_2 and converts to iron oxide forming "islands" of elemental sulfur via:

$$4FeS + 3O_2 \Leftrightarrow 2Fe_2O_3 + 4S \tag{85}$$

or

$$3FeS + 3O_2 \Leftrightarrow Fe_3O_4 + 3S \tag{86}$$

- alternatively, at very high H_2S concentration, the following reaction can occur to give elemental sulfur:

$$H_2S \Leftrightarrow H_2 + S \tag{87}$$

Localized corrosion by elemental sulfur can occur due to:

- direct reaction with the iron in the steel:

$$S + Fe \Leftrightarrow FeS \tag{88}$$

- or first leads to formation of sulfuric acid via:

$$4S + 4H_2O \Leftrightarrow 3H_2S + H_2SO_4 \tag{89}$$

which then attacks the steel.

A more in-depth discussion about the corrosion mechanisms of mild steel involving elemental sulfur exceeds the scope of this review.

3.3 Calculation of Mild Steel H_2S Corrosion Rate

3.3.1 Pure H_2S aqueous environment

Due to the presence of the inner mackinawite film and the outer porous sulfide layer, it is assumed that the corrosion rate of steel in H_2S solutions is always under mass transfer control. One can then write the flux of H_2S due to:

- convective diffusion through the mass transfer boundary layer:

$$Flux_{H_2S} = k_{m(H_2S)}\left(c_{H_2S} - c_{o(H_2S)}\right) \tag{90}$$

- molecular diffusion through the liquid in the porous outer sulfide layer:

$$Flux_{H_2S} = \frac{D_{H_2S}\varepsilon\psi}{\delta_{os}}\left(c_{o(H_2S)} - c_{i(H_2S)}\right) \tag{91}$$

- solid state diffusion through the inner mackinawite film:

$$Flux_{H_2S} = A_{H_2S}\ln\left(\frac{c_{i(H_2S)}}{c_{s(H_2S)}}\right) \tag{92}$$

In a steady state, the three fluxes are equal to each other and are equivalent to the corrosion rate:

$$CR_{H_2S} = Flux_{H_2S} M_{Fe} / \rho_{Fe} \tag{93}$$

further corrected for appropriate corrosion rate unit.

By eliminating the unknown interfacial concentrations $c_{o(H_2S)}$ and $c_{i(H_2S)}$ from equations (90) to (92), the following equation is obtained for the flux (corrosion rate) due to H_2S:

$$Flux_{H_2S} = A_{H_2S} \ln \frac{c_{H_2S} - Flux_{H_2S}\left(\frac{\delta_{os}}{D_{H_2S}\varepsilon\psi} + \frac{1}{k_{m(H_2S)}}\right)}{c_{s(H_2S)}} \tag{94}$$

This is an algebraic nonlinear equation with respect to $Flux_{H_2S}$ which does not have an explicit solution but can be solved by using a simple numerical algorithm such the interval halving method or similar. These are available as ready-made routines in spreadsheet applications or in any common computer programming language. The prediction for $Flux_{H_2S}$ depends on a number of constants used in the model which can be either found in handbooks (such as D_{H_2S}), calculated from the established theory (e.g. $k_{m(H_2S)}$) or are determined from experiments (e.g. $A_{H_2S}, c_{s(H_2S)}$). The unknown thickness of the outer sulfide layer change with time and need to be calculated as described below.

It is assumed that the amount of layer retained on the metal surface at any point in time depends on the balance of:

- layer formation kinetics (as the layer is generated by spalling of the thin mackinawite film underneath it and by precipitation from the solution), and
- layer damage kinetics (as the layer is damaged by intrinsic or hydrodynamic stresses and/or by chemical dissolution):

$$\underbrace{SRR}_{\substack{\text{sulfide layer}\\ \text{retention}\\ \text{rate}}} = \underbrace{SFR}_{\substack{\text{sulfide layer}\\ \text{formation}\\ \text{rate}}} - \underbrace{SDR}_{\substack{\text{sulfide layer}\\ \text{damage}\\ \text{rate}}} \tag{95}$$

where all the terms are expressed in kmol/(m^{2}s). In order to simplify the calculations it can be assumed that in the typical range of application (4<pH<7), precipitation and dissolution of ferrous sulfide layer do not play a significant role, so it can be written:

$$SRR = CR - SDR_m \tag{96}$$

Even in stagnant conditions about half of the sulfide layer that forms is lost from the steel surface due to intrinsic growth stresses by internal cracking and spalling, i.e. $SDR_m \approx 0.5\,CR$, so one can write finally:

$$SRR = 0.5\,CR \tag{97}$$

i.e. about half of the iron corroded is found on the steel surface in the form of ferrous sulfide. More experimentation is required to determine how the mechanical layer damage is affected by hydrodynamic forces.

Once the layer retention rate *SRR* is known, the change in mass of the outer sulfide layer can be easily calculated as:

$$\Delta m_{os} = SRR \; M_{FeS} \; A \; \Delta t \tag{98}$$

The porosity of the outer sulfide layer was determined to be very high ($\varepsilon \approx 0.9$) by comparing the weight of the layer with the cross-sectional SEM images showing its thickness. On the other hand this layer has proven to be rather protective (i.e. impermeable to diffusion) which can only be explained by its low tortuosity arising from its layered structure. By comparing the measured and calculated corrosion rates in the presence of the outer sulfide layer, the tortuosity factor was calculated to be $\psi = 0.003$.

A time-marching explicit solution procedure could now be established where:

1. the corrosion rate $Flux_{H_2S}$ in the absence of outer sulfide layer can be calculated by using equation (94), and assuming $\delta_{os} = 0$,
2. the amount of sulfide layer Δm_{os} formed over a time interval Δt is calculated by using equation (98),
3. the new corrosion rate $Flux_{H_2S}$ in the presence of sulfide layer can be recalculated by using equation (94),
4. a new time interval Δt is set and steps 2 and 3 repeated.

At very low H_2S gas concentrations (ppm_w range), there is very little dissolved H_2S and the corrosion rate is directly affected by pH. A mackinawite layer still forms and

controls the corrosion rate, however the corrosion process is largely driven by the reduction of H^+ ions, rather than of H_2S. In an analogy with the approach laid out above, the following expression is obtained for the flux of H^+ ions controlled by the presence of the ferrous sulfide layers:

$$Flux_{H^+} = A_{H^+} \ln \frac{c_{H^+} - Flux_{H^+}\left(\frac{\delta_{os}}{D_{H^+}\varepsilon\psi} + \frac{1}{k_{m(H^+)}}\right)}{c_{s(H^+)}} \tag{99}$$

The flux $Flux_{H^+}$ is directly related to the corrosion rate by H^+ ions:

$$CR_{H^+} = Flux_{H^+}\frac{M_{Fe}}{\rho_{Fe}} \tag{100}$$

further corrected for the appropriate corrosion rate unit.

By solving equations (94) and (99) sequentially in time, the total corrosion rate in mixed pure H_2S aqueous environments can be calculated as:

$$CR = CR_{H_2S} + CR_{H^+} \tag{101}$$

3.3.2 Mixed CO_2/H_2S Environments

For mild steel corrosion in CO_2/H_2S containing environments, one can account for the effect of CO_2 by following the same assumptions. A similar expression can be

obtained for the corrosion rate driven by the presence of CO_2 and controlled by the presence of the ferrous sulfide layers:

$$Flux_{CO_2} = A_{CO_2} \ln \frac{c_{CO_2} - Flux_{CO_2}\left(\frac{\delta_{os}}{D_{CO_2}\varepsilon\psi} + \frac{1}{k_{m(CO_2)}}\right)}{c_{s(CO_2)}} \tag{102}$$

The flux $Flux_{CO_2}$ is equivalent to the corrosion rate by CO_2:

$$CR_{CO_2} = Flux_{CO_2} \frac{M_{Fe}}{\rho_{Fe}} \tag{103}$$

further corrected for appropriate corrosion rate unit.

By solving equations (94), (99) and (102), the total corrosion rate in mixed CO_2/H_2S environments can be calculated as:

$$CR = CR_{H_2S} + CR_{H^+} + CR_{CO_2} \tag{104}$$

3.3.3 Mixed $CO_2/HAc/H_2S$ Environments

IF both HAc and CO_2 exist in the H_2S containing environment, the corrosion rate induced by the presence of HAc can be obtained in the similar fashion as those for H_2S and CO_2:

$$Flux_{HAc} = A_{HAc} \ln \frac{c_{HAc} - Flux_{HAc}\left(\frac{\delta_{os}}{D_{HAc}\varepsilon\psi} + \frac{1}{k_{m(HAc)}}\right)}{c_{s(HAc)}} \tag{105}$$

The flux $Flux_{HAc}$ is equivalent to the corrosion rate by:

$$CR_{HAc} = Flux_{HAc} \frac{M_{Fe}}{\rho_{Fe}} \tag{106}$$

further corrected for appropriate corrosion rate unit.

By solving equations (94), (99), (102) and (105), the total corrosion rate in mixed $CO_2 / HAc / H_2S$ environments can be calculated as:

$$CR = CR_{H_2S} + CR_{H^+} + CR_{CO_2} + CR_{HAc} \tag{107}$$

3.4 Limitations of modeling of aqueous H_2S corrosion of mild steel

The calculation model presented above covers uniform H_2S , CO_2 / H_2S and $CO_2 / HAc / H_2S$ corrosion. There are numerous limitations:

- It does not predict localized corrosion in either environment.
- While it covers a very broad range of H_2S partial pressures it is not recommended to use this model below p_{H_2S}=0.01 mbar or above p_{H_2S}=10bar. Similar limits apply to the CO_2 partial pressure. This leaves a very broad area of applicability for the present model.

- This H_2S model does not account for any precipitation of ferrous sulfide, ferrous carbonate, or any other scale; therefore in cases where this is deemed important for corrosion, the model should be used with caution. The model also does not account for various transformations of sulfide layer from one type to another which are known to happen over time.
- The present model does not account for dissolution of the sulfide layer that may occur at very low pH. Therefore the use of this model at pH<3 is not recommended. Similarly the model should be used with caution for pH>7 where it has not been tested.
- The model does not account for the effect of high chloride concentrations, oxygen, elemental sulfur or any other unspecified condition which is known to affect the corrosion rate and is not explicitly covered in the theoretical underpinnings of the present model.

While this calculation model is clearly not inclusive of all the important processes in aqueous H_2S corrosion of mild steel, it is believed that the main underlying assumptions about the formation and protective nature of a mackinawite layer are correct. The comparison of the performance of this model with experimental data is given in the section below which covers the main factors affecting CO_2/H_2S corrosion of mild steel.

3.5 Key Factors Affecting Aqueous H_2S Corrosion of Mild Steel

3.5.1 Effect of H_2S partial pressure

Corrosion rate of mild steel at extremely low H_2S partial pressures is seen in Figure where in atmospheric glass cell experiments p_{H_2S} ranged from 0.0013 – 0.32 mbar, corresponding to 1 – 250 ppm_m in the gas phase at 1 bar CO_2. Clearly this is a CO_2 dominated corrosion scenario (p_{CO_2} / p_{H_2S} ratio is in the range 10^3 – 10^6), however the presence of H_2S controls the corrosion rate. Even when present in such minute amounts, H_2S reduces the pure CO_2 (H_2S-free) corrosion rate by 3 to 10 times due to formation of a thin mackinawite film. The model presented above successfully captures this effect as shown in Figure 15.

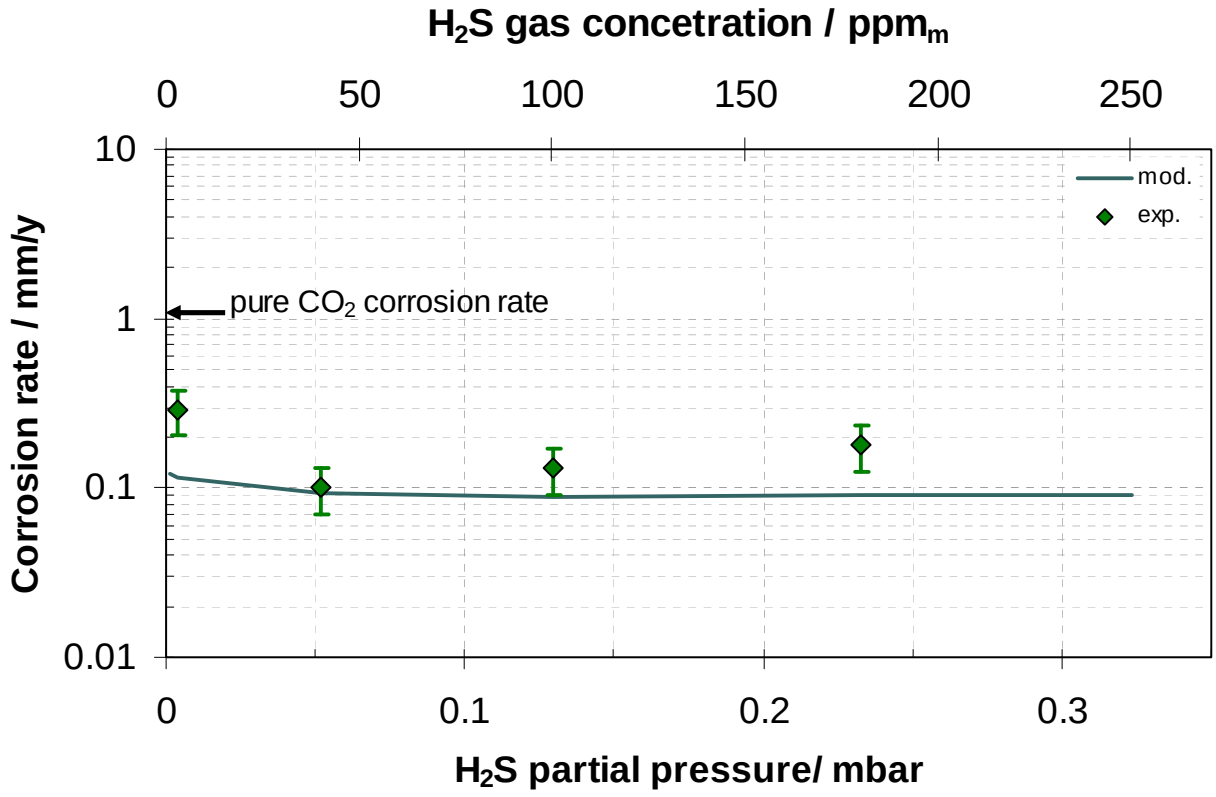

Figure 15. The corrosion rate vs. partial pressure of H_2S; experimental data (exp.) = points, model predictions (mod.) = lines; conditions: total pressure p=1 bar, p_{CO_2} =1 bar, p_{H_2S} = 0.0013 – 0.32 mbar, T=20°C, reaction time 24 hours, pH 5, 1000 rpm. For reference: pure CO_2 corrosion rate is measured to be 1 mm/y. Data taken form Lee[38].

At higher H_2S partial pressures the same effect is observed as shown in Figure 16, which shows results from autoclave experiments conducted at a very high total pressure (p=138 bar) and a high CO_2 partial pressure (p_{CO_2} =13.8 bar). When comparing the predictions with the experimental results it can be seen that the model underpredicts the observed rate of steel corrosion by approximately a factor of two. However, when this is compared with a pure CO_2 (H_2S -free) corrosion rate under the same conditions (which is not reported but can be predicted at almost 20 mm/y) the accuracy of the model can be considered as reasonable. At the highest p_{CO_2} / p_{H_2S} ratio of 3500 (p_{CO_2} =13.8 bar, p_{H_2S} =40 mbar), CO_2 accounts for approximately 70% of the corrosion rate and 30% can be ascribed to H_2S. At the lowest p_{CO_2} / p_{H_2S} ratio of 1180 (p_{CO_2} =13.8 bar, p_{H_2S} =116 mbar), CO_2 accounts for approximately 57% of the corrosion rate and 43% can be ascribed to H_2S.

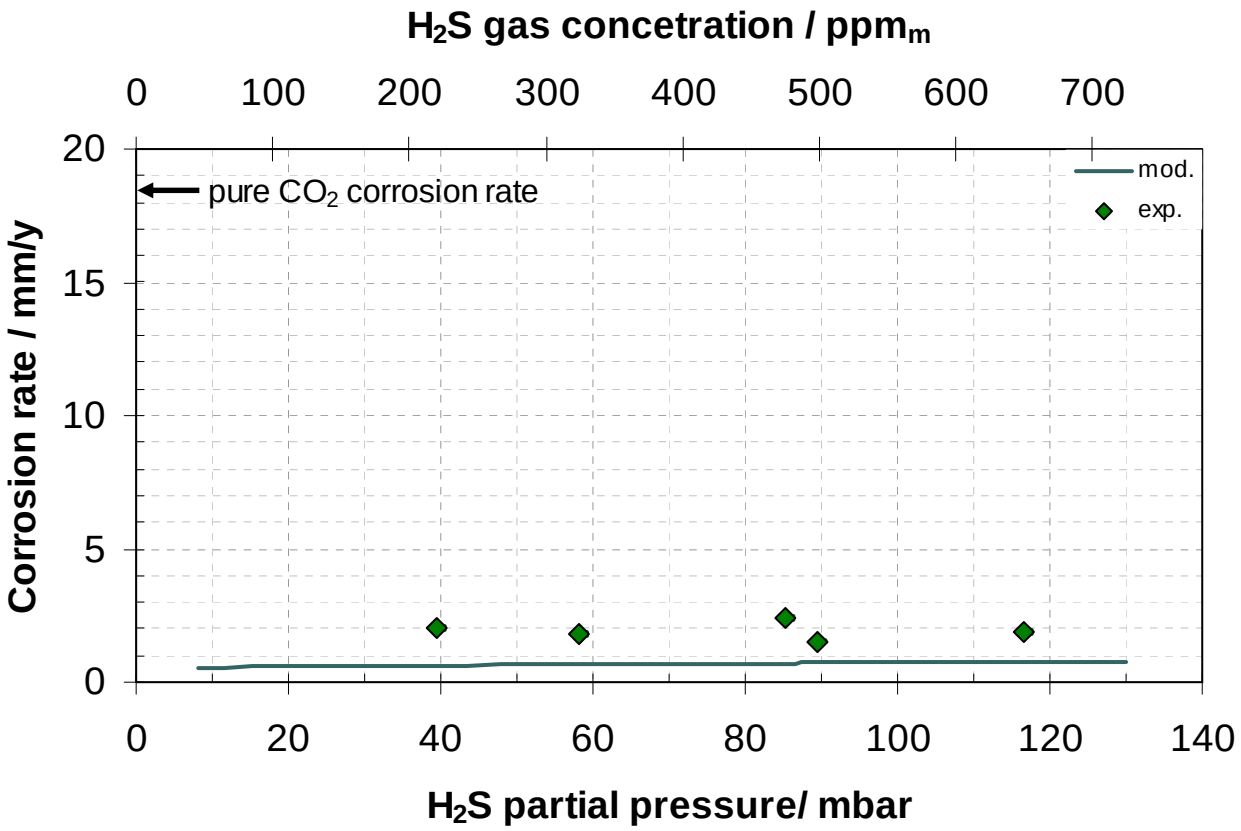

Figure 16. The corrosion rate vs. H_2S partial pressure; experimental data (exp.) = points, model predictions (mod.) = lines; conditions: total pressure p=137.9 bar, p_{CO_2} =13.8 bar, p_{H_2S} = 40 – 120 mbar, T=50°C, experiment duration 3 days, pH 4.0 – 6.2, stagnant. Experimental data taken from Smith and Pacheco et al. [31]

Corrosion rates of mild steel at very high partial pressures of H_2S (p_{H_2S}=3 – 20 bar) and CO_2 (p_{CO_2}=3 – 12.8 bar) for exposures lasting up to 4 days are shown in Figure 17. This is a situation where the H_2S was the dominant corrosive species. At the highest p_{CO_2} / p_{H_2S} ratio of 1.8 (p_{CO_2}=5.3 bar, p_{H_2S}=3 bar) H_2S generated approximately 86% of the corrosion rate. At the lowest p_{CO_2} / p_{H_2S} ratio of 0.2 (p_{CO_2}=4 bar, p_{H_2S}=20 bar) H_2S generated 97% of the overall corrosion rate. It is also noted that the model predictions show that the corrosion rate in the first reaction hour is on average 20 mm/y with an

initial corrosion rate of 60 mm/y and a final corrosion rate of 10 mm/y. Concededly, the pitting corrosion rate was reported to be 30 mm/y in a field case with similar conditions, which is related to the very high, H_2S -driven corrosion seen at the beginning of experiments before a thick protective ferrous sulfide film forms.

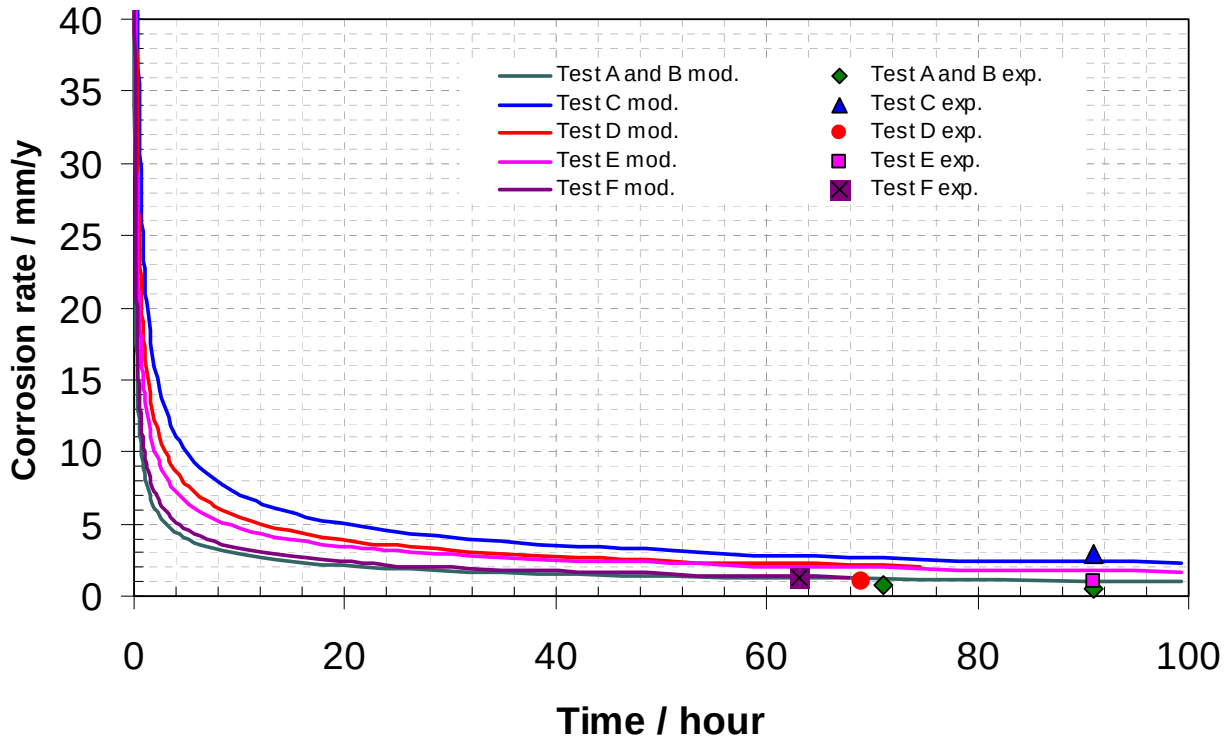

Figure 17. The corrosion rate vs. time; experimental data (exp.) = points, model predictions (mod.) = lines; Test A and B: p=8.3 bar, p_{CO_2} =5.3 bar, p_{H_2S} =3 bar, T=60°C, 71hours (A) and 91 hours (B); Test C: p=24 bar, p_{CO_2} =4 bar, p_{H_2S} =20 bar, T=70°C, 91 hours; Test D: p=15.7 bar, p_{CO_2} =3.5 bar, p_{H_2S} =12.2 bar, T=65°C, 69 hours; Test E: p=20.8 bar, p_{CO_2} =12.8 bar, p_{H_2S} =8 bar, T=65°C, 91 hours; Test F: p=7.2 bar, p_{CO_2} =3 bar, p_{H_2S} =4.2 bar, T=65°C, 63 hours; experimental data taken from Bich and Goerz[40]

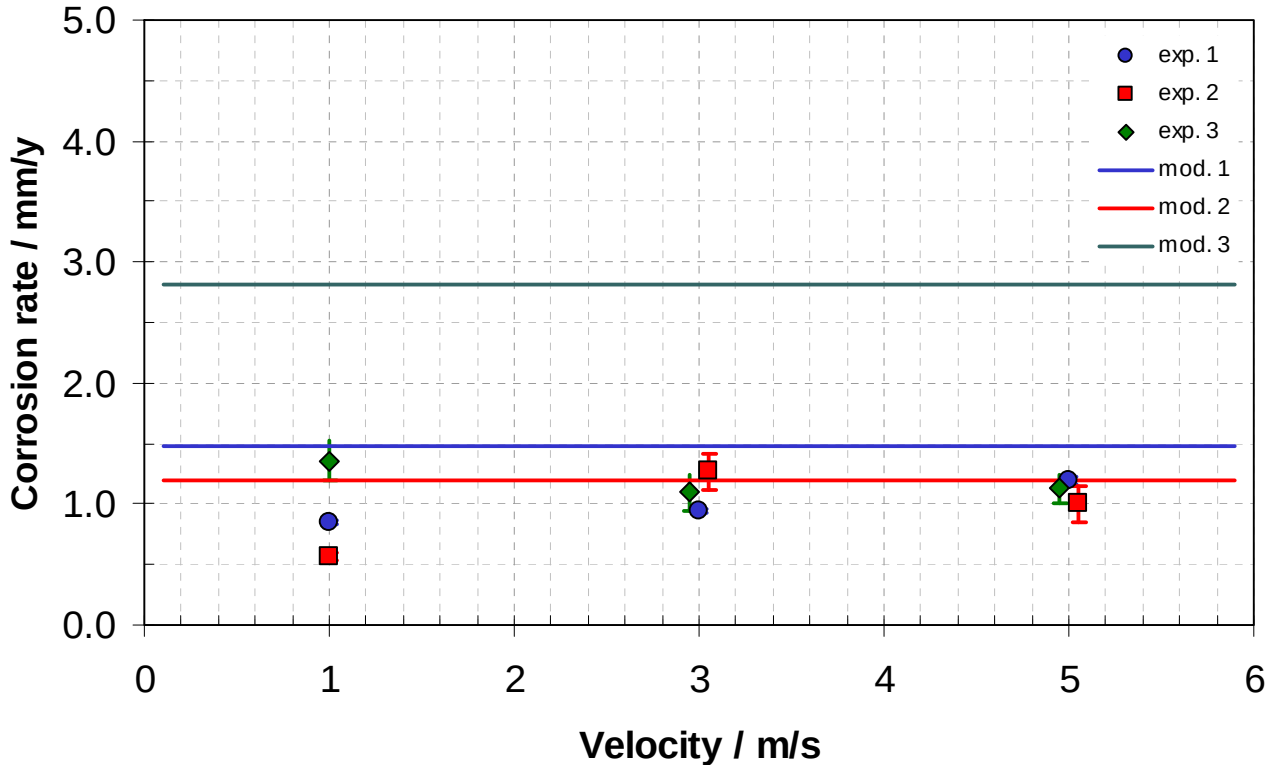

Figure 18. The corrosion rate vs. velocity; experimental data (exp.) = points, model predictions (mod.) = lines; exp 1.: 19 days, p=40 bar, p_{CO_2} =3.3 bar, p_{H_2S} =10 bar, T=80°C, pH 3.1, v=1 – 5 m/s; exp 2.: 21 days, p=40 bar, p_{CO_2} =3.3 bar, p_{H_2S} =10 bar, T=25°C, pH 3.2, v=1 – 5 m/s; exp 3.: 10 days, p=40 bar, p_{CO_2} =10 bar, p_{H_2S} =30 bar, T=80°C, pH 2.9, v=1 – 5 m/s; experimental data taken from Omar et al.[41]

3.5.2 Effect of time

A marked decrease of pure CO_2 corrosion rate due to the presence of H_2S with time is seen in stratified pipe flow as shown in Figure 19. This is clearly a mixed CO_2/H_2S corrosion scenario. At a p_{CO_2}/p_{H_2S} ratio of 200 (p_{CO_2} =2 bar, p_{H_2S} =4 mbar) the CO_2 contribution to the corrosion rate is 75% with most of the balance provided by H_2S. At the p_{CO_2}/p_{H_2S} ratio of 28 (p_{CO_2} =2 bar, p_{H_2S} =70 mbar) both CO_2 and H_2S account for approximately 50% of the overall corrosion rate.

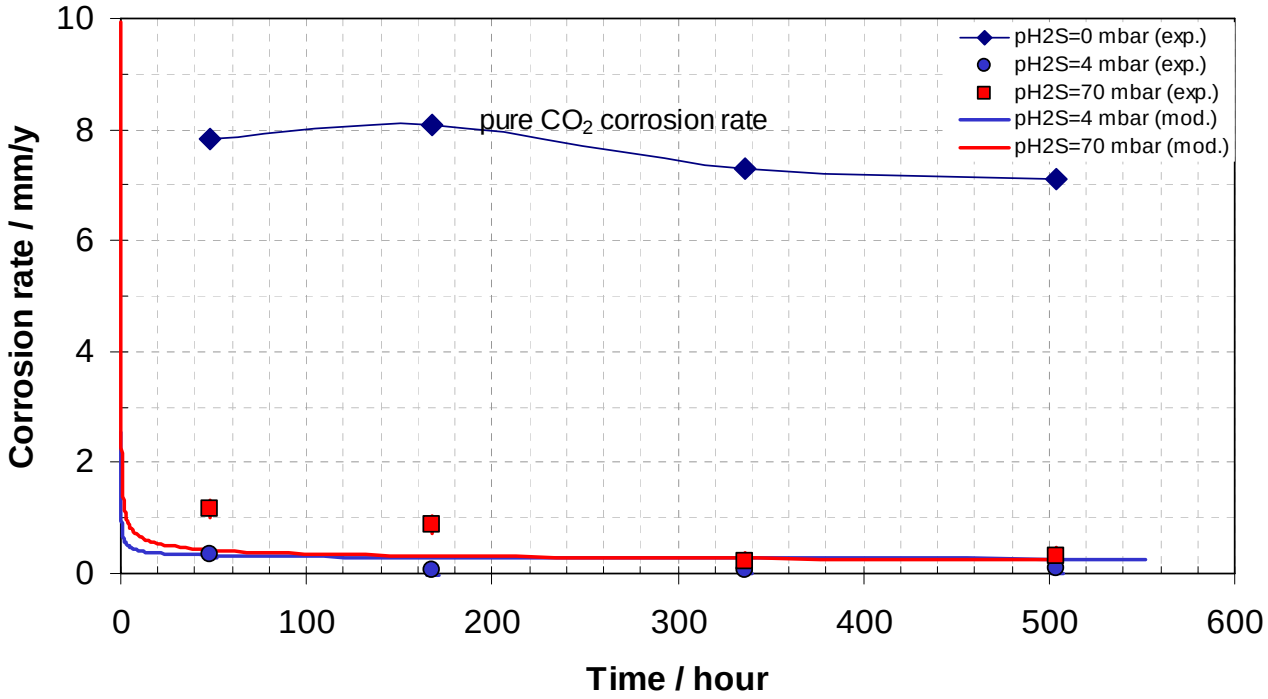

Figure 19. The corrosion rate vs. time; experimental data (exp.) = points, model predictions (mod.) = lines; conditions: total pressure p=3 bar, p_{CO_2} =2 bar, p_{H_2S} = 3 – 70 mbar, T=70°C, experiment duration 2 – 21 days, pH 4.2 – 4.9, liquid velocity 0.3 m/s. Experimental data taken from Singer et al. [39]

Corrosion experiments at high temperature (120°C), high partial pressures of CO_2 (p_{CO_2} =6.9 bar) and H_2S (p_{H_2S} =1.38 – 4.14 bar) in exposures lasting up to 16 days are shown in Figure 20. A steadily decreasing corrosion rate was observed due to buildup of a protective ferrous sulfide layer. The effect of p_{H_2S} increase on corrosion rate was very small and practically vanished over time. Both these effects were readily captured by the model with very good accuracy as seen in Figure 20. In this case the H_2S is the dominant corrosive species. At the highest p_{CO_2} / p_{H_2S} ratio of 5 (p_{CO_2} =6.9 bar, p_{H_2S} =1.38 bar) H_2S generated approximately 70% of the corrosion rate. At the

lowest p_{CO_2} / p_{H_2S} ratio of 1.67 (p_{CO_2} =6.9 bar, p_{H_2S} =4.14 bar) H_2S generated 82% of the overall corrosion rate.

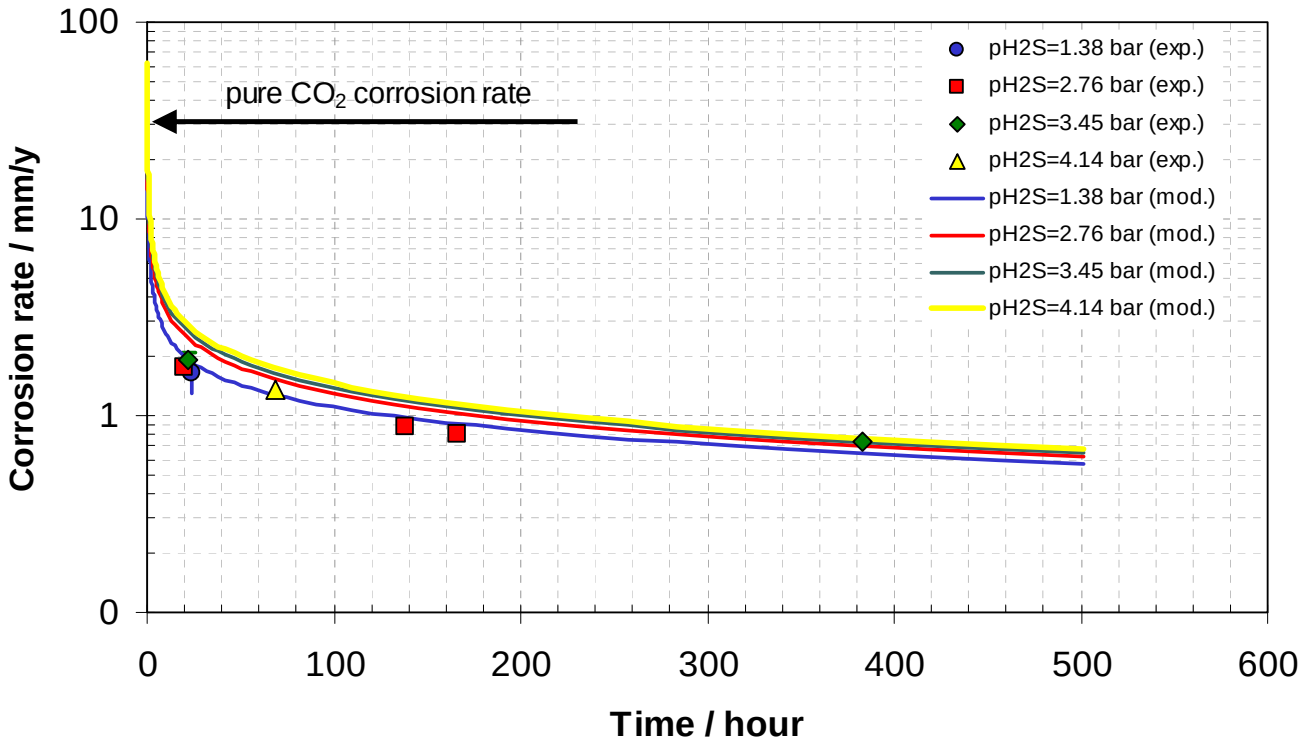

Figure 20. The corrosion rate vs. time; experimental data (exp.) = points, model predictions (mod.) = lines; conditions: total pressure p=7 bar, p_{CO_2} =6.9 bar, p_{H_2S} = 1.38 – 4.14 bar, T=120°C, experiment duration 1 – 16 days, pH 3.95 – 4.96, liquid velocity 10 m/s. Experimental data taken from Kvarekval et al.[42]

The longest H_2S containing corrosion experiments which are practically achievable in the lab are of the order of a few weeks or at best a few months, while predictions are meant to cover a period of at least a few decades, in order to be meaningful. With this in mind it is interesting to take the experimental conditions above (p_{CO_2} =6.9 bar, p_{H_2S} =3.45 bar, T=120°C, pH 4, v=10 m/s) and extend the simulation to 25 years. The result is shown in Figure 21. The corrosion rate was predicted to start out rather high

as observed in the experiments, however it was reduced to below 0.1 mm/y after 2 years and was as low as 0.03 mm/y after 25 years. The average corrosion rate over this period was only 0.06 mm/y, which amounts to a wall thickness loss of only 1.5 mm over the 25 years, an acceptable amount by any practical account. Actually most of the other conditions simulated have shown that rather low H_2S uniform corrosion rates are obtained for very long exposures, which agrees with general field experience as recently discussed by Bonis et al.[33] Nevertheless, no quantitative long term lab data are currently available to backup these long term predictions.

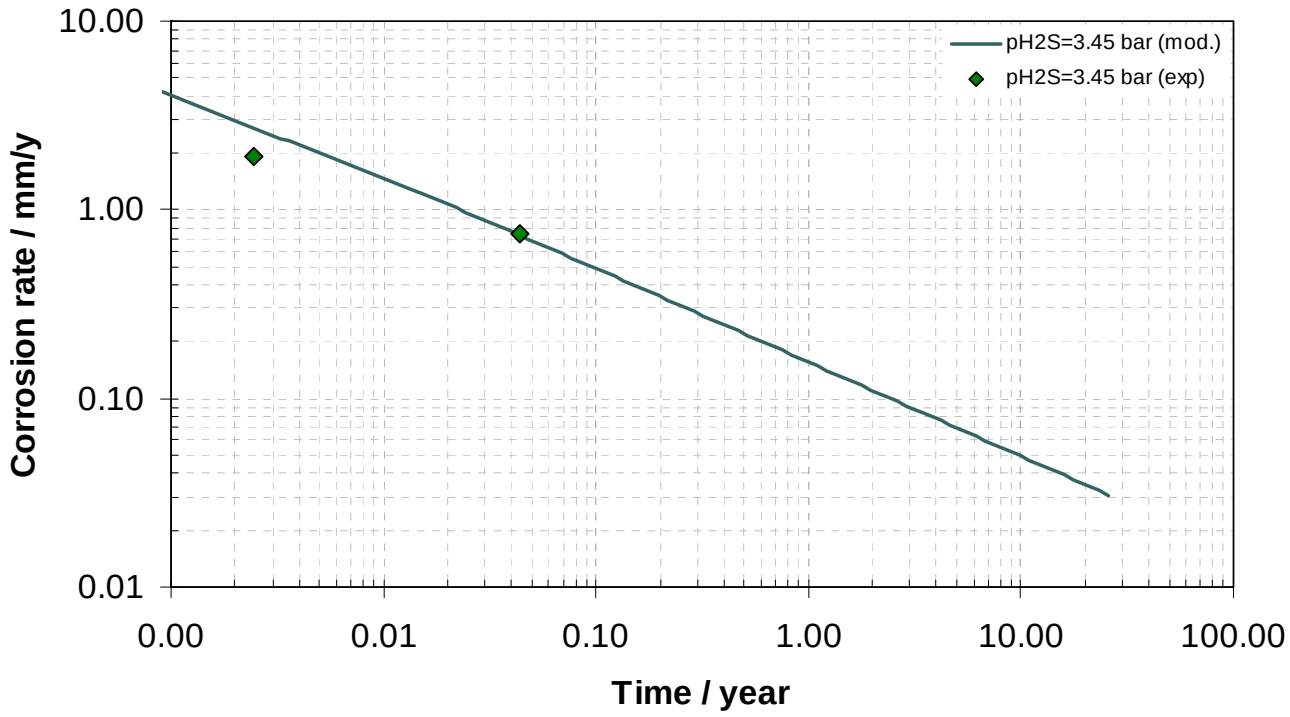

Figure 21. Extension of corrosion prediction to a 25-year lifetime; experimental (points), predicted (lines); conditions: p_{CO_2} =6.9 bar, p_{H_2S} =3.45 bar, T=120°C, pH 4, liquid velocity 10 m/s; taken from Kvarekval *et al.* [42]

3.6 Localized H_2S Corrosion of Mild Steel in Aqueous Solutions

Localized H_2S corrosion of mild steel is even less understood than its uniform counterpart. While it is not very common, anecdotal evidence exists that has linked localized H_2S corrosion in aqueous environments to other factors such as: high chloride content, the presence of elemental sulfur and the transformation of one type of sulfide into another. Intense research of these topics is ongoing with breakthrough in understanding expected in the decade to come.

4 NOMENCALTURE

A surface area of the steel in m²

A/V surface to volume ratio in 1/m

$A_{(FeCO_3)}$ constant in the Arrhenius-type equation for $k_{r(FeCO_3)}$

A_{H_2S} solid state diffusion kinetic constant for H_2S through mackinawite film,

$A_{H_2S} = 2.0 \cdot 10^{-5}$ mol/(m²s)

A_{H^+} solid state diffusion kinetic constant for H^+ through mackinawite film,

$A_{H^+} = 4.0 \cdot 10^{-4}$ mol/(m²s)

A_{HAc} solid state diffusion kinetic constant for HAc through mackinawite film,

$A_{HAc} = 2.0 \cdot 10^{-6}$ mol/(m²s)

A_{CO_2} solid state diffusion kinetic constant for CO_2 through mackinawite film,

$A_{CO_2} = 2.0 \times 10^{-6}$ mol/(m²s)

$b_{a(Fe)}$ anodic Tafel slope for Fe oxidation in V

$b_{c(H^+)}$ cathodic Tafel slope for H^+ ion reduction in V

$b_{c(HAc)}$ cathodic Tafel slope for HAc ion reduction in V

$b_{c(H_2CO_3)}$ cathodic Tafel slope for H_2CO_3 reduction in V

$b_{c(O_2)}$ cathodic Tafel slope for O_2 reduction in V

$b_{c(H_2O)}$ cathodic Tafel slope for H_2O reduction in V

$B_{(FeCO_3)}$ constant in the Arrhenius-type equation for $k_{r(FeCO_3)}$ in kJ/kmol

c_{CO_2} bulk aqueous concentration of CO_2 in kmol/m³

$c_{CO_3^{2-}}$ bulk aqueous concentration of CO_3^{2-} ions in kmol/m³

$c_{Fe^{2+}}$ bulk aqueous concentration of Fe^{2+} ions in kmol/m^3

c_{H^+} bulk aqueous concentration of H^+ ions in kmol/m^3

$c_{s(H^+)}$ "near-zero" concentration of H^+ underneath the mackinawite film at the steel surface, set to $1.0 \cdot 10^{-7}$ in kmol/m^3

c_{HAc} bulk aqueous concentration of undissociated HAc in kmol/m^3

$c_{HAc,ref}$ bulk aqueous concentration of HAc under reference conditions in kmol/m^3

c_{O_2} bulk aqueous concentration of O_2 in kmol/m^3

$c_{s(HAc)}$ "near-zero" concentration of HAc underneath the mackinawite film at the steel surface, set to $1.0 \cdot 10^{-7}$ in kmol/m^3

$c_{HCO_3^-}$ bulk aqueous concentration of HCO_3^- ions in kmol/m^3

$c_{H_2CO_3}$ bulk aqueous concentration of H_2CO_3 in kmol/m^3

$c_{H_2CO_3}$ bulk aqueous concentration of H_2CO_3 in kmol/m^3

c_{H_2S} bulk aqueous concentration of H_2S in kmol/m^3

c_{HS^-} bulk aqueous concentration of HS^- ions in kmol/m^3

c_i bulk aqueous concentration of a given aqueous species in kmol/m^3

$c_{i(H_2S)}$ aqueous concentration of H_2S at the inner sulfide film/outer sulfide layer interface in kmol/m^3

$c_{S^{2-}}$ bulk aqueous concentration of S^{2-} ions in kmol/m^3

$c_{s(H_2S)}$ "near-zero" aqueous concentration of H_2S underneath then mackinawite film at the steel surface, set to $1.0 \cdot 10^{-7}$ in kmol/m^3

$c_{o(H_2S)}$ aqueous concentration of H_2S at the outer sulfide layer/solution interface in kmol/m^3

$c_{s(CO_2)}$ aqueous concentration of CO_2 underneath then mackinawite film at the steel surface

CR corrosion rate in mm/y

d characteristic dimension for a given flow geometry in m

d_p diameter of a pipe in m

d_c diameter of a rotating cylinder in m

D diffusion coefficient of a given species in m²/s

D_{H^+} aqueous diffusion coefficient for H^+ in m²/s

$D_{ref(H^+)}$ reference aqueous diffusion coefficient for H^+,

$D_{ref(H^+)} = 9.31 \times 10^{-9}$, in m²/s at 25°C

D_{HAc} aqueous diffusion coefficient for HAc in m²/s

$D_{ref(HAc)}$ reference aqueous diffusion coefficient for HAc,

$D_{ref(HAc)} = 5.0 \times 10^{-10}$, in m²/s at 25°C

$D_{H_2CO_3}$ aqueous diffusion coefficient of H_2CO_3 in m²/s

$D_{ref(H_2CO_3)}$ reference aqueous diffusion coefficient of H_2CO_3,

$D_{ref,H_2CO_3} = 1.3 \cdot 10^{-9}$ m²/s at 25°C

D_{O_2} aqueous diffusion coefficient for O_2 in m²/s

$D_{ref(O_2)}$ reference aqueous diffusion coefficient for O_2,

$D_{ref(O_2)} = 2.0 \times 10^{-9}$, in m²/s at 25°C

D_{H_2S} aqueous diffusion coefficient for dissolved H_2S in m²/s

D_{CO_2} aqueous diffusion coefficient for dissolved CO_2,

$D_{CO_2} = 1.96 \times 10^{-9}$, in m²/s

E potential in V

E_{corr} corrosion (open circuit) potential in V

$E_{rev(Fe)}$ reversible potential of Fe oxidation, $E_{rev(Fe)}$ = - 0.488 V

$E_{rev(H^+)}$ reversible potential for H^+ ion reduction in V

$E_{rev(HAc)}$ reversible potential for HAc ion reduction in V

$E_{rev(H_2CO_3)}$ reversible potential for H_2CO_3 reduction in V

$E_{rev(O_2)}$ reversible potential for O_2 reduction in V

$E_{rev(H_2O)}$ reversible potential for H_2O reduction in V

$f_{H_2CO_3}$ flow factor for the chemical reaction boundary layer

F Faraday constant: F =96,485 C/mol$_e$

$Flux_{H_2S}$ flux of H_2S in kmol/(m^{2}s)

$Flux_{H^+}$ flux of H^+ ions in kmol/(m^{2}s)

$Flux_{HAc}$ flux of HAc ions in kmol/(m^{2}s)

$Flux_{CO_2}$ flux of CO_2 in mol/(m^{2}s)

$H_{sol(CO_2)}$ Henry's constant for dissolution of CO_2 in bar/(kmol/m^3)

ΔH_{Fe} activation enthalpy for Fe oxidation, ΔH_{Fe}=50 kJ/mol

$\Delta H_{(H^+)}$ activation enthalpy for H^+ ion reduction, $\Delta H_{(H^+)}$=30 kJ/mol

$\Delta H_{(HAc)}$ activation enthalpy for HAc reduction, $\Delta H_{(HAc)}$=55 kJ/mol

$\Delta H_{(H_2CO_3)}$ activation enthalpy for H_2CO_3 reduction, $\Delta H_{(H_2CO_3)}$=57.5 kJ/mol

$\Delta H_{(O_2)}$ activation enthalpy for O_2 reduction, $\Delta H_{(O_2)}$=10 kJ/mol

$\Delta H_{(H_2O)}$ activation enthalpy for H_2O reduction, $\Delta H_{(H_2O)}$=30 kJ/mol

i current density in A/m^2

i_{corr} corrosion current density in A/m^2

$i_{a(Fe)}$ anodic current density of iron oxidation in A/m^2

$i_{c(H^+)}$ cathodic current density for H^+ ion reduction in A/m^2

$i_{c(HAc)}$ cathodic current density for HAc reduction in A/m^2

$i_{c(H_2CO_3)}$ cathodic current density for H_2CO_3 reduction in A/m^2

$i_{c(O_2)}$ cathodic current density for O_2 reduction in A/m^2

$i_{c(H_2O)}$ cathodic current density for H_2O reduction in A/m^2

$i^d_{\lim(H^+)}$ mass transfer (diffusion) limiting current density for H^+ ion reduction in A/m^2

$i^d_{\lim(HAc)}$ mass transfer (diffusion) limiting current density for HAc reduction in A/m^2

$i^r_{\lim(H_2CO_3)}$ chemical reaction limiting current density for H_2CO_3 reduction in A/m^2

$i^d_{\lim(O_2)}$ mass transfer (diffusion) limiting current density for O_2 reduction in A/m^2

$i_{o(Fe)}$ exchange current density of iron oxidation in A/m^2

$i_{o(H^+)}$ exchange current density for H^+ ion reduction in A/m^2

$i_{o(HAc)}$ exchange current density for HAc ion reduction in A/m^2

$i_{o(H_2CO_3)}$ exchange current density for H_2CO_3 reduction in A/m^2

$i_{o(O_2)}$ exchange current density for O_2 reduction in A/m^2

$i_{o(H_2O)}$ exchange current density for water reduction in A/m^2;

$i^{ref}_{o(Fe)}$ reference exchange current density of Fe oxidation, $i^{ref}_{o(Fe)}$= 1 A/m^2

$i^{ref}_{o(H^+)}$ reference exchange current density of H^+ oxidation,

$i^{ref}_{o(H^+)}$ = 0.03 A/m^2 at $T_{c,ref}$ =25°C and pH 4

$i_{o(H_2CO_3)}^{ref}$ reference exchange current density for H_2CO_3 reduction,

$i_{o(H_2CO_3)}^{ref}$ = 0.06 A/m² at $T_{c,ref}$ =25°C, pH5, and $c_{H_2CO_3,ref}$ =10^{-4} kmol/m³

$i_{o(HAc)}^{ref}$ reference exchange current density for HAc reduction,

$i_{o(HAc)}^{ref}$ = 0.1 A/m² at $T_{c,ref}$ =20°C and $c_{HAc_3,ref}$ =10^{-3} kmol/m³

$i_{o(O_2)}^{ref}$ reference exchange current density for O_2 reduction,

$i_{o(O_2)}^{ref}$ = 0.06 A/m² at $T_{c,ref}$ =25°C

$i_{o(H_2O)}^{ref}$ reference exchange current density for H_2O reduction in A/m²,

$i_{o(H_2O)}^{ref} = 3 \cdot 10^{-5}$ A/m² at $T_{c,ref}$ =25°C

$i_{\alpha(H^+)}$ charge transfer current density for H^+ ion reduction in A/m²

$i_{\alpha(H_2CO_3)}$ charge transfer current density for H_2CO_3 reduction in A/m²

$i_{\alpha(O_2)}$ charge transfer current density for O_2 reduction in A/m²

I ionic strength in kmol/m³

k_{hyd}^{b} backward reaction rate of H_2CO_3 dehydration reaction in 1/s, $k_{hyd}^{b} = k_{hyd}^{f} / K_{hyd}$

k_{hyd}^{f} forward reaction rate for the CO_2 hydration reaction in 1/s

$k_{m(H^+)}$ aqueous mass transfer coefficient for H^+ in m/s

$k_{m(H_2CO_3)}$ aqueous mass transfer coefficient for H_2CO_3 in m/s

$k_{m(HAc)}$ aqueous mass transfer coefficient for HAc in m/s

$k_{m(O_2)}$ aqueous mass transfer coefficient for O_2 in m/s

$k_{m(H_2S)}$ aqueous mass transfer coefficient for H_2S in m/s

$k_{m(CO_2)}$ aqueous mass transfer coefficient for CO_2 in m/s

$k_{r(FeCO_3)}$ kinetic constant in the ferrous carbonate precipitation rate equation in 1/(mol s)

K_{hyd} equilibrium hydration constant for CO_2, $K_{hyd} = k^f_{hyd} \big/ k^b_{hyd} = 2.58 \cdot 10^{-3}$

K_{bi} equilibrium constant for dissociation of HCO_3^- in kmol/m³

K_{bs} equilibrium constant for dissociation HS^- in kmol/m³

K_{ca} equilibrium constant for dissociation of H_2CO_3 in kmol/m³

K_{hs} equilibrium constant for dissociation H_2S in kmol/m³

$K_{sol(H_2S)}$ solubility constant for dissolution of H_2S in (kmol/m³/bar)

$K_{sol(CO_2)}$ solubility constant for dissolution of CO_2 in (kmol/m³/bar)

$K_{sp(FeCO_3)}$ solubility product constant for ferrous carbonate in (kmol/m³)²

$K^{mackin}_{sp(FeS)}$ solubility product constant for mackinawite in (kmol/m³)²

m_{os} mass of the outer sulfide layer in kg

M_{Fe} molecular mass of iron in kg/kmol$_{Fe}$

M_{FeS} molecular mass of ferrous sulfide in kg/mol$_{FeS}$,

n number of electrons used in reducing or oxidizing a given species in kmol$_e$/kmol

p_{CO_2} partial pressure of CO_2 in bar

p_{H_2S} partial pressure of H_2S in bar

$\Re$ electrochemical reaction rate in kmol/(m² s)

$\Re_{FeCO_3}$ precipitation rate for iron carbonate in kmol/(m³ s)

R universal gas constant, $R = 8.314$ J/(mol K)

Re Reynolds number, $Re = v\rho_{H_2O}\, d \big/ \mu_{H_2O}$

Sc Schmidt number of a given species, $Sc = \mu_{H_2O} / \left(\rho_{H_2O} D \right)$

Sh_p Sherwood number of a given species for a straight pipe flow geometry,

$$Sh_p = k_m \, d_p / D$$

Sh_r Sherwood number of a given species for a rotating cylinder flow geometry,

$$Sh_r = k_m \, d_c / D$$

$SS_{(FeCO_3)}$ supersaturation of iron carbonate

ST scaling tendency

T_c temperature in °C

$T_{c,ref}$ reference temperature, $T_{c,ref}$ =25°C

T_f temperature in °F

T_k temperature in K

v water characteristic velocity in m/s

z_i species charge of various aqueous species

Greek characters

$\delta_{m\,(H_2CO_3)}$ thickness of the mass transfer layer for H_2CO_3 in m

$\delta_{r\,(H_2CO_3)}$ thickness of the chemical reaction layer for H_2CO_3 in m

δ_{os} is the thickness of the outer sulfide layer in m, $\delta_{os} = m_{os} / \left(\rho_{FeS} \, A \right)$

Δt time interval in s

$\mu_{\mathrm{H_2O}}$ water dynamic viscosity in $Pa \cdot s$

$\mu_{\mathrm{H_2O},ref}$ reference water dynamic viscosity $Pa \cdot s$ at a reference temperature,

$$\mu_{\mathrm{H_2O},ref} = 1.002 \times 10^{-4} \; Pa \cdot s \text{ at } 20^{\circ}\mathrm{C}$$

$\zeta_{H_2CO_3}$ ratio of the mass transfer layer and chemical reaction thicknesses for H_2CO_3

ε is the outer sulfide layer porosity

ψ is the outer sulfide layer tortuosity factor

ρ_{H_2O} density of water in kg/m^3

ρ_{Fe} density of iron in kg/m^3

ρ_{FeS} density of ferrous sulfide in kg/m^3

5 REFERENCES

1. M. R. Bonis and J. L. Crolet, "Basics of the Prediction of the Risks of CO_2 Corrosion in Oil and Gas Wells", Corrosion/89, paper no. 466, (Houston, TX: NACE International, 1989).

2. J. Oddo and M. Tomson, "Simplified calculation of $CaCO_3$ saturation at high temperatures and pressures in brine solutions", SPE of AIME (Richardson, TX: Society of Petroleum Engineers, 1982), 1583-1590.

3. D. A. Palmer, R. van Eldik, Chem. Rev., 83, (1983): p. 651.

4. W. Sun, S. Nešić, R.C. Woollam, "The Effect of Temperature and Ionic Strength on Iron Carbonate ($FeCO_3$) Solubility Limit", to appear in Corrosion Science, 2008.

5. W. Sun, S. Nešić, "Kinetics of Corrosion Layer Formation, Part 1. Iron Carbonate Layers in Carbon Dioxide Corrosion", Corrosion, Vol. 64, (2008): p. 334.

6. D. M. Drazic, "Iron and its Electrochemistry in an Active State", Aspects of Electrochemistry, Vol 19, p.79, Plenum Press, 1989.

7. W. Lorenz and K Heusler, "Anodic Dissolution of Iron Group Metals", in Corrosion Mechanisms, ed. F. Mansfeld, Marcel Dekker, New York, 1987.

8. S. Nešić, N. Thevenot, and J. L. Crolet, "Electrochemical Properties of Iron Dissolution in CO_2 solutions - basics revisited", Corrosion/96, paper no. 3, (Houston, TX: NACE International, 1996).

9. C. de Waard and D. E. Milliams, Corrosion, 31 (1975): p.131.

10. L. G. S. Gray, B. G. Anderson, M. J. Danysh, P. G. Tremaine, "Mechanism of Carbon Steel Corrosion in Brines Containing Dissolved Carbon Dioxide at pH 4", Corrosion/89, paper no. 464, (Houston, TX: NACE International, 1989).

11. E. Eriksrud and T. Søntvedt, "Effect of Flow on CO_2 Corrosion Rates in Real and Synthetic Formation Waters", Advances in CO_2 Corrosion, Vol. 1. Proceedings of the Corrosion /83 Symposium on CO_2 Corrosion in the Oil and Gas Industry, Editors: R. H. Hausler, H. P. Goddard, p.20, (Houston, TX: NACE, 1984).

12. G. Schmitt and B. Rothman, Werkstoffe und Korrosion, 28 (1977): p.816.

13. L. G. S. Gray, B. G. Anderson, M. J. Danysh and P. R. Tremaine, "Effect of pH and Temperature on the Mechanism of Carbon Steel Corrosion by Aqueous Carbon Dioxide", Corrosion/90, paper no. 40, (Houston, TX: NACE International, 1990).

14. P. Delahay, J. Am. Chem. Soc., 74 (1952): p.3497.

15. S. Nešić, J. Postlethwaite and S. Olsen, "An Electrochemical Model for Prediction of CO_2 Corrosion", Corrosion/95, paper no. 131, (Houston, TX: NACE International, 1995).

16. S. Nešić, B. F. M. Pots, J. Postlethwaite and N. Thevenot, "Superposition of Diffusion and Chemical Reaction Limiting Currents - Application to CO_2 Corrosion", Journal of Corrosion Science and Engineering, Vol.1, Paper No. 3, World Wide Web, http://www.cp.umist.ac.uk/JCSE/Vol1/PAPER3/V1_p3int.htm, The Corrosion Information Server, The Corrosion & Protection Centre at UMIST, Manchester, UK, 1995.

17. K. Chokshi, W. Sun and S. Nešić, "Iron Carbonate Film Growth and the Effect of Inhibition in CO_2 Corrosion of Mild Steel", Corrosion/05, paper no. 285, (Houston, TX: NACE International, 2005).

18. Y. Sun, S. Nešić,, "A Parametric Study and Modeling on Localized CO_2 Corrosion in Horizontal Wet Gas Flow". CORROSION/2004, Paper No. 380 (Houston, TX: NACE International, 2004).

19. S. Nešić, G.T. Solvi, and J. Enerhaug,, Corrosion, 51 (1995) p. 773.

20. Y. Sun, K. George, S. Nešić, "The Effect of Cl^- and Acetic Acid on Localized CO_2 Corrosion in Wet Gas Flow", CORROSION/2003, Paper No. 3327, (Houston, TX: NACE International 2003).

21. Y.M. Gunaltun, D. Larrey, "Correlation of Cases of Top of Line Corrosion With Calculated Water Condensation Rates", CORROSION/2000, Paper No. 71, (Houston, TX: NACE International 2000).

22. F. Vitse, S. Nešić, Y. Gunaltun, D. Larrey de Torreben, P. Duchet-Suchaux, "Mechanistic Model for the Prediction of Top-of-the-Line Corrosion Risk", Corrosion, Vol. 59, (2003): p. 1075.

23. A. Anderko, R. Young, "Simulation of CO_2 / H_2S Corrosion Using Thermodynamic and Electrochemical Models", CORROSION/99, paper no. 31, (Houston, TX: NACE International, 1999).

24. C. de Waard and U. Lotz, "Prediction of CO_2 Corrosion of Carbon Steel", Corrosion/93, paper no. 69, (Houston, TX: NACE International, 1993).

25. F.P. Berger, K.-F.F.-L. Hau, Int. J. Heat Mass Transfer, v.20, p. 1185, 1977.

26. M. Eisenberg, C. W. Tobias and C. R.Wilke, J. of Electrochem. Soc., 101, (1954): p. 306.

27. D. W. Shoesmith, P. Taylor, M. G. Bailey, & D. G. Owen, J. Electrochem. Soc., The formation of ferrous monosulfide polymorphs during the corrosion of iron by aqueous hydrogen sulfide at 21 °C, 125 (1980) 1007-1015.

28. D. W. Shoesmith, Formation, transformation and dissolution of phases formed on surfaces, Lash Miller Award Address, Electrochemical Society Meeting, Ottawa, Nov. 27, 1981.

29. S. N. Smith, A proposed mechanism for corrosion in slightly sour oil and gas production, Twelfth International Corrosion Congress, Houston, Texas, September 19 – 24, paper no. 385, 1993.

30. S. N. Smith and E. J. Wright, Prediction of minimum H_2S levels required for slightly sour corrosion, Corrosion/94, Paper no. 11, NACE International, Houston, Texas, 1994.

31. S. N. Smith and J. L. Pacheco, Prediction of corrosion in slightly sour environments, Corrosion/2002, paper no. 02241, NACE International, Houston, Texas, 2002.

32. S. N. Smith and M. Joosten, Corrosion of carbon steel by H_2S in CO_2 containing oilfield environments, Corrosion/2006, Paper no. 06115, NACE International, Houston, Texas, 2006.

33. M. Bonis, M. Girgis, K. Goerz, and R. MacDonald, Weight loss corrosion with H_2S : using past operations for designing future facilities, Corrosion/2006, paper no. 06122, NACE International, Houston, Texas, 2006.

34. Suleimenov, O. M.; Krupp, R. E., Geochimica et Cosmochimica Acta 1994, 58, 2433-2444.

35. Kharaka, Y.K.; Perkins, E.H.; Gunter, W.D.; Debral, J.D.; Bamford, C.H., "Solmineq 88: A Computer Program for Geochemical Modeling of Water Rock Interactions" (Menlo Park, CA: Alberta Research Council, 1989).

36. Benning, L. G.; Wilkin, R. T.; Barnes, H. L., Chemical Geology 2000, 167, 25-51.

37. A. Criaud, C. Fouillac and B. Marty, "Low enthalpy geothermal fluids from the paris basin. 2—Oxidation-reduction state and consequences for the prediction of corrosion and sulfide scaling," Geothermics, Vol. 18, Issues 5-6, 711-727, (1989).

38. K. J. Lee, A mechanistic modeling of CO_2 corrosion of mild steel in the presence of H_2S, PhD dissertation, Ohio University, 2004.

39. M. Singer, B. Brown, A. Camacho, and S. Nešić, Combined effect of CO_2, H_2S and acetic acid on bottom of the line corrosion, paper no. 07661, NACE International, Houston, Texas, 2007.

40. N. N. Bich and K. Goerz, Caroline pipeline failure: findings on corrosion mechanisms in wet sour gas systems containing significant CO_2, paper no. 26, NACE International, Houston, Texas, 1996.

41. I. H. Omar, Y. M. Gunaltun, J. Kvarekval and A. Dugstad, H_2S corrosion of carbon steel under simulated Kashagan field conditions, paper no. 05300, NACE International, Houston, Texas, 2005.

42. J. Kvarekval, R. Nyborg, and H. Choi, Formation of multilayer iron sulfide films during high temperature CO_2/H_2S corrosion of carbon steel, paper no. 03339, NACE International, Houston, Texas, 2003.